HHS Public Access

Author manuscript

Prog Neurobiol. Author manuscript; available in PMC 2024 May 01.

Published in final edited form as:

Prog Neurobiol. 2023 May ; 224: 102436. doi:10.1016/j.pneurobio.2023.102436.

Spinal astrocytic MeCP2 regulates Kir4.1 for the maintenance of chronic hyperalgesia in neuropathic pain

Mengchan Ou[a,#], **Yali Chen**[a,b,#], **Jin Liu**[a,b], **Donghang Zhang**[a,b], **Yaoxin Yang**[a,b], **Jiefei Shen**[d], **Changhong Miao**[e], **Shao-Jun Tang**[f], **Xin Liu**[f], **Daniel K. Mulkey**[c], **Tao Zhu**[a,*], **Cheng Zhou**[b,*]

[a]Department of Anesthesiology, West China Hospital of Sichuan University, Chengdu, 610041, China

[b]Laboratory of Anesthesia and Critical Care Medicine, National-Local Joint Engineering Research Centre of Translational Medicine of Anesthesiology, West China Hospital of Sichuan University, Chengdu, 610041, China

[c]Departments of Physiology and Neurobiology, University of Connecticut, Storrs, Connecticut, 06269, USA

[d]Laboratory of Oral Diseases & National Clinical Research Center for Oral Diseases and Department of Prosthodontics, West China Stomatology Hospital of Sichuan University, Chengdu 610041, China

[e]Department of Anesthesiology, Zhongshan Hospital, Fudan University, Shanghai, 200032, China

[f]Department of Anesthesiology and The Stony Brook University Pain and Analgesia Research Center (SPARC), Stony Brook University, Stony Brook, New York 11794, USA

Abstract

Astrocyte activation in the spinal dorsal horn may play an important role in the development of chronic neuropathic pain, but the mechanisms involved in astrocyte activation and their modulatory effects remain unknown. The inward rectifying potassium channel protein 4.1 (Kir4.1) is the most important background K^+ channel in astrocytes. However, how Kir4.1 is regulated and

* Correspondence to: Dr. Cheng Zhou, Laboratory of Anesthesia and Critical Care Medicine, National-Local Joint Engineering Research Centre of Translational Medicine of Anesthesiology, West China Hospital of Sichuan University, Chengdu, 610041, China, zhouc@163.com, Dr. Tao Zhu, Department of Anesthesiology, West China Hospital of Sichuan University, Chengdu, 610041, China, xwtao.zhu@foxmail.com.

#Equal contributors.

Author contributions

Conceptualization: M.O. and C.Z.; Data curation: M.O. and Y.C.; Formal analysis: M.O., Y.C., C.Z. and D.Z.; Funding acquisition: M.O., C.Z., Y.C. and S.J.T.; Investigation: D.Z. Y.Y. and J.S.; Methodology: M.O., Y.C. and D.Z.; Project administration: M.O., Y.C. and X.L.; Resources: J.L., J.S., C.M., S.J.T. D.K.M. and T.Z.; Software: M.O. and Y.C; Supervision: J.L., D.K.M., T.Z. and C.Z.; Validation: J.L., D.Z. and Y.Y.; Visualization: M.O. and Y.C.; Writing - original draft: M.O. and Y.C.; Writing - review & editing: D.K.M., S.J.T. and C.Z.

Declarations of interest: none.

Competing interests

The authors report no conflict of interest.

contributes to behavioral hyperalgesia in chronic pain is unknown. In this study, single-cell RNA sequencing analysis indicated that the expression levels of both Kir4.1 and Methyl-CpG-binding protein 2 (MeCP2) were decreased in spinal astrocytes after chronic constriction injury (CCI) in a mouse model. Conditional knockout of the Kir4.1 channel in spinal astrocytes led to hyperalgesia, and overexpression of the Kir4.1 channel in spinal cord relieved CCI-induced hyperalgesia. Expression of spinal Kir4.1 after CCI was regulated by MeCP2. Electrophysiological recording in spinal slices showed that knockdown of Kir4.1 significantly up-regulated the excitability of astrocytes and then functionally changed the firing patterns of neurons in dorsal spinal cord. Therefore, targeting spinal Kir4.1 may be a therapeutic approach for hyperalgesia in chronic neuropathic pain.

Keywords

Astrocyte activation; Chronic neuropathic pain; Kir4.1; MeCP2; Neuronal sensitization

1. Introduction

Neuropathic pain (nerve pain) is a debilitating and difficult to treat condition that often develops into a state of long-lasting chronic pain (Finnerup, Kuner, & Jensen, 2021). It is estimated that 2 billion people globally (25% of the world population) suffer from chronic pain (Goldberg & McGee, 2011), with the prevalence increasing as the risk factors associated with this condition, including old age and diabetes, become more frequent in the population (Colloca et al., 2017). Chronic pain is also associated with other serious problems such as depression, anxiety and sleep disorders (Cohen & Mao, 2014; Naranjo et al., 2019) and is a leading contributor to the ongoing opioid epidemic (Skolnick, 2018). Not surprisingly, the economic cost of chronic pain is tremendous; estimates based on health care costs and lost productivity reach $635 billion per year in the USA (Gaskin & Richard, 2012). Therefore, chronic pain is a health crisis with enormous clinical, social and economic burdens. Despite this, cellular and molecular mechanisms contributing to the maintenance of chronic pain are poorly understood; consequently, effective long-term treatment options are lacking.

Key elements of the pain circuitry are well known and include neurons in the dorsal horn of the spinal cord that relay sensory information from the periphery to higher brain regions for pain perception (Wercberger, Braz, Weinrich, & Basbaum, 2021). However, neural activity is subject to modulation by other cells, including astrocytes, and recent evidence suggests that dorsal horn astrocytes also contribute to pain signaling. For example, in the absence of injury, spinal astrocytes have been shown to limit pain sensory transduction by releasing purinergic-adenosine or anti-inflammatory cytokines (Sommer, Leinders, & Üçeyler, 2018; Wahlman et al., 2018). However, following injury, astrocytes in the dorsal horn proliferate (gliosis) and transition into a pro-inflammatory state characterized by release of excitatory cytokines (so called reactive astrocytes) that serve to increase pain sensitivity (Gao & Ji, 2010). Furthermore, in the absence of injury or disease, selective optogenetic activation of spinal astrocytes also causes gliosis and increases pain sensitivity (Nam et al., 2016). These results identify astrocytes as important modulators of pain sensitivity. However, the

mechanisms by which astrocytes contribute to maintenance of chronic neuropathic pain remain unclear.

Inward rectifying potassium channel 4.1 proteins (Kir4.1) are preferentially expressed by astrocytes where they regulate membrane potential and serve as conduits for K^+ uptake from the extracellular space; as such, these channels are determinants of several astrocyte processes, including regulation of extracellular K^+ and glutamate (MacAulay, 2020). Considering that dysregulation of extracellular K^+ and glutamate is expected to increase neural activity, it is perhaps not surprising that K^+ channel activators show analgesic potential for treatment of chronic pain (Tsantoulas & McMahon, 2014) and that loss of Kir4.1 function is associated with development of neuropathic pain. For example, the expression and functions of Kir4.1 channels were decreased in dorsal root ganglion satellite glial cells in a rat model of neuropathic pain (Vit, Ohara, Bhargava, Kelley, & Jasmin, 2008; H. Zhang et al., 2009), and knockdown of Kir4.1 from satellite glial cells resulted in pain-like behaviors in freely behaving rats (Vit et al., 2008). These results indicate that Kir4.1 plays an important role in the hyperalgesia of neuropathic pain. However, it is not clear how astrocytic Kir4.1 expression changes as neuropathic pain develops, and the mechanisms by which loss of Kir4.1 contributes to manifestation of pain are poorly understood.

Methyl-CpG-binding protein 2 (MeCP2) is a transcription factor that regulates gene expression (including *Kcnj10*, the gene encoding Kir4.1 (Kahanovitch et al., 2018)) and is involved in neuronal survival, differentiation, and maintenance of synaptic function (Chang, Khare, Dani, Nelson, & Jaenisch, 2006; Fukuda, Itoh, Ichikawa, Washiyama, & Goto, 2005; Smrt et al., 2007). MeCP2 is widely expressed, including by both neurons and astrocytes (Ballas, Lioy, Grunseich, & Mandel, 2009; Kifayathullah et al., 2010; Zachariah, Olson, Ezeonwuka, & Rastegar, 2012). Diminished expression of MeCP2 in neurons is associated with diminished pain sensitivity(Suzuki, Shinoda, Honda, Shirakawa, & Iwata, 2016). However, it is not clear how loss of MeCP2 from astrocytes impacts pain sensitivity. A previous study showed that MeCP2-deficient mice expressed less Kir4.1 mRNA and protein, and astrocytes from these animals showed diminished Kir4.1-like current (Kahanovitch et al., 2018). These results suggest MeCP2 is a positive transcriptional regulator of Kir4.1 (Kahanovitch et al., 2018). However, the roles of MeCP2 in neuropathic pain remain elusive, in part because MeCP2 expression varies in a region- and cell-type-specific manner following nerve injury (Géranton, Fratto, Tochiki, & Hunt, 2008; Géranton, Morenilla-Palao, & Hunt, 2007; Tao et al., 2020; Tochiki, Cunningham, Hunt, & Géranton, 2012; R. Zhang et al., 2015; Z. Zhang et al., 2014) and few studies have investigated cell-type-specific roles of MeCP2 in the development and maintenance of neuropathic pain.

Here, we test the hypothesis that reduced expression of Kir4.1 channels in astrocytes contributes to hyperalgesia in a mouse model of chronic neuropathic pain, and in an MeCP2-deficient mouse model. We show that MeCP2 regulation of Kir4.1 expression in astrocytes is necessary and sufficient for the maintenance of hyperalgesia in chronic neuropathic pain. These results suggest that astrocytic Kir4.1 channels should be a high-priority therapeutic target for chronic neuropathic pain.

2. Materials and methods

2.1 Animals

The study protocols were approved by the Animal Ethics Committee of West China Hospital of Sichuan University (Chengdu, China), and were conducted in accordance with the Animal Research Reporting *In vivo* Experiments (ARRIVE) guidelines. Neonatal (postnatal days 12–14, both sexes) C57BL/6 J mice, adult (~ 8 weeks, both sexes) C57BL/6 J mice, Kir4.1$^{f/f}$ mice and GFAP$^{Cre\text{-}ERT2}$ mice were used. C57BL/6 J mice were purchased from Chengdu Dassy Biological Technology Co. Ltd (Chengdu, China). Kir4.1 conditional knockout in astrocytes (Kir4.1 cKO) mice were crossbred from a transgenic B6. Cg-Tg (GFAP-Cre) 77.6Mvs/2J line and recombinant Kir4.1 floxed (Kir4.1$^{f/f}$) line. From postnatal days 28, the Kir4.1 cKO mice were intraperitoneally injected with tamoxifen 1 mg once a day for 4 consecutive days. Then Kir4.1 cKO mice were obtained 21 days after the last injection. The control mice were homologous Kir4.1 non-knockout (Kir4.1$^{+/+}$) mice. GFAP$^{Cre\text{-}ERT2}$ mice and Kir4.1$^{f/f}$ mice were obtained from Dr. Ken McCarthy (Univ. North Carolina)). All the mice were housed, 5 per cage, under standard conditions (22–24°C, humidity 45–55% and lights on from 7:00 to 19:00), with ad libitum access to food and water. Neonatal mice were kept with their mothers.

2.2 CCI model

Neuropathic pain was induced by chronic constriction injury (CCI) of the sciatic nerve (Bennett & Xie, 1988). Briefly, mice were anesthetized with 2% isoflurane. Then, the left sciatic nerve was exposed at the mid-thigh level and loosely ligated (5–0 chromic gut) with 4 ties (at 1-mm intervals). The ligation strength was sufficient to cause slight shrinkage of the left posterior limb. The right side was used as the CCI-contralateral side: the sciatic nerve was only exposed but not ligated.

2.3 Pain behavior tests

Von-Frey filaments test was used to measure mechanical allodynia (Liu, Liu, Song, & Song, 2013). The mice were placed individually in a Plexiglas chamber on an elevated metal mesh floor and acclimated for 30 min. The plantar surface of the hind limb was stimulated with a series of Von-Frey filaments (0.008 g, 0.02 g, 0.04 g, 0.07 g, 0.16 g, 0.4 g, 0.6 g, 1 g, 1.4 g, 2 g, 4 g, 6 g, 8 g, 10 g and 15 g). The absolute withdrawal threshold was determined using the up-down method (Dixon, 1991). Hargreaves test was used to measure thermal allodynia (Hargreaves, Dubner, Brown, Flores, & Joris, 1988). The mice were acclimated in the same chambers on an elevated transparent glass platform. Following 30 min acclimation, the plantar surface of the hind limb was exposed to a radiant beam through the transparent glass. The radiant heat was shut off when hind paw movement occurred or after 20 s to prevent tissue damage. The thermal stimuli were repeated 3 times at 10-min intervals, and the mean latency was calculated to assess thermal hyperalgesia. All the behavioral tests were performed between 9:00 am and 5:00 pm.

2.4 Intrathecal injection

Mice were anesthetized with 2% isoflurane, and then restrained in the horizontal position. A 25-G needle connected to a Hamilton syringe was inserted into the subarachnoid space between L5-L6. A sudden flick of the tail was used as an indicator of successful puncture into the subarachnoid space (Zhou et al., 2015). The needle was held in place for at least 60 s after the injection to avoid an outflow. The virus solution (Tailtool Bioscience, Shanghai, China) was injected into the subarachnoid space (5 μL for adult mice).

Kir4.1-siRNA (5'-ACAAAGGAGGGTGAGAATATT-3') and control-siRNA (5'-UUCUCCGAACGUGUCACGUTT-3') were dissolved in RNase-free water. *In vivo* SilenceMag™ transfection reagent (OZ Biosciences, Marseille, France) was mixed with Kir4.1-siRNA or control-siRNA to a final concentration of 1 μg/μL before injection. Then, Kir4.1-siRNA or control-siRNA was injected into the subarachnoid space of neonatal mice in a volume of 2 μL.

2.5 Real-time PCR (RT-PCR)

Mice were anesthetized with 2% isoflurane and then the spinal lumbar enlargements (L4-L6) were rapidly removed. Total RNA was isolated using the Eastep® Super RNA extraction kit (Promega, Shanghai, China). Reverse transcription was performed with a GoScript™ Reverse Transcription Kit (Promega, Shanghai, China). RT-PCR was performed using TaqMan™ Fast Advanced Master Mix (Thermo Fisher Scientific, USA) and TaqMan specific probes (all from Life Sciences) for Kcnj10 (Kir4.1, Mm00445028_m1), MeCP2 (MeCP2, Mm01193537_g1) and GAPDH (GAPDH, Mm99999915_g1) (Thermo Fisher Scientific, USA) according to the manufacturer's protocols. The relative fold change of gene expression was calculated with the $2^{-\Delta\Delta Ct}$ method using GAPDH as the internal control.

2.6 Western blot

Mice were anesthetized with 2% isoflurane and then the spinal lumbar enlargements (L4-L6) were rapidly removed and homogenized. The protein concentration was determined with a BCA protein assay kit (Beyotime, Shanghai, China). The protein was electrophoresed on a 7.5% sodium dodecyl sulfate polyacrylamide gel and then transferred to polyvinyl difluoride (PVDF) membranes (Bio-Rad, Hercules, CA, USA). The PVDF membranes were incubated overnight at 4°C with primary antibodies against Kir4.1 (1:1000, rabbit, Alomone Labs, Jerusalem, Israel), MeCP2 (1:500, rabbit, Abcam, Cambridge, UK), glial fibrillary acidic protein (GFAP) (1:5000, Proteintech, Wuhan, China) and β-actin (1:5000, mouse, Abcam, Cambridge, UK). Next, the membranes were incubated with the secondary antibody (1:4,000, Cell Signaling Technology, Beverly, MA, USA) at ambient temperature for 2 h. The protein bands were visualized using enhanced chemiluminescence and the intensities of the bands were quantified using Image J software (National Institutes of Health, Bethesda, MD, USA).

2.7 Immunofluorescence staining

Mice were deeply anesthetized with 2% isoflurane and then transcardially perfused with phosphate-buffered saline (PBS) (pH 7.4) followed by 4% paraformaldehyde in PBS (pH 7.4). The spinal lumbar enlargements were removed and soaked in 4% formalin overnight

at 4°C and then in 30% sucrose until the tissue sank to the bottom. The spinal cords were cut into 12-μm thick sequential sections using a freezing microtome (CM1850; Leica, Buffalo Grove, IL, USA). Sections were labeled by overnight incubation at 4°C with primary antibodies: rabbit anti-Kir4.1 extracellular peptide (1:400, Alomone Labs, Jerusalem, Israel), rabbit anti-MeCP2 (1:500, Abcam, Cambridge, UK), guinea pig anti-GFAP (1:1000, Synaptic Systems, Germany), mouse anti-Myelin Basic Protein (MBP) (1:400, Abcam, Cambridge, UK) and mouse anti-NeuN (1:500, Abcam, Cambridge, UK). Fluorescent secondary antibodies were added to 5% bovine serum albumin and incubated for 2 h at room temperature: Alexa Fluor 488 goat anti-mouse IgG (1:500, Jackson Immuno Research, West Grove, PA, USA), Alexa Fluor 488 goat anti-guinea pig IgG (1:500, Abcam, Cambridge, UK), and Cy^{TM3} goat anti-rabbit IgG (1:500, Jackson Immuno Research, West Grove, PA, USA). Fluorescent images were acquired using a Zeiss AxioImager Z.2 (Guangzhou, China).

2.8 Preparation of acute spinal cord slices

Mice (P14) were anesthetized with ketamine/xylazine (60/10 mg/kg). Then, the spinal lumbar enlargements were removed, fixed in agar rose gel (2%) and initially mounted on a vibratome (VT1000 A, Leica). Sagittal spinal cord slices (250–300 μm thick) were cut in ice-cold artificial cerebrospinal fluid (aCSF) containing (in mM): 260 sucrose, 3 KCl, 5 $MgCl_2$, 1 $CaCl_2$, 1.25 NaH_2PO_4, 26 $NaHCO_3$, 10 glucose and 1 kynurenic acid. Slices were incubated in external solution containing (in mM): 130 NaCl, 3 KCl, 2 $MgCl_2$, 2 $CaCl_2$, 1.25 NaH_2PO_4, 26 $NaHCO_3$ and 10 glucose at 37 °C for 30 min and then maintained at room temperature (24–26°C) for another 30 min prior to an experiment. The aCSF and incubation solutions were equilibrated with 95% O_2 / 5% CO_2. After incubation, spinal cord slices were mounted in the recording chamber to permit electrophysiological recordings at room temperature.

2.9 Electrophysiology

Each spinal cord slice was mounted in a recording chamber and submerged in continuously perfused incubation solution (~2 mL/min), bubbled with 95% O_2 / 5% CO_2. Dorsal spinal cord (lamina I-II) neurons were visualized and identified by their shapes using infrared differential interference contrast microscopy. Electrophysiological recordings were made using an Axopatch 700B amplifier and a Digidata 1440 digitizer linked to a computer running pClamp 10.2 software (Molecular Devices, Sunnyvale, CA, USA). Recordings were sampled at 20 kHz and filtered at 10 kHz in the whole-cell configuration. Whole-cell voltage-clamp and current-clamp recordings were established using internal solution containing (mM): 120 KCH_4SO_3, 4 NaCl, 1 $MgCl_2$, 0.5 $CaCl_2$, 10 HEPES, 10 EGTA, 3 Mg-ATP, 0.3 GTP-Tris at pH 7.2. Holding potentials were −80 mV and −60 mV for astrocytes and neurons, respectively. For astrocytic recordings, holding currents and conductance were sampled every 15 s and current-voltage (I-V) relationships were determined using voltage steps between −40 mV and −150 mV. To record neuronal firing behavior currents were injected into the neurons of spinal lamina I and II from −120 pA to 150 pA (30 pA steps) with 1-s durations. As previously described (Ruscheweyh & Sandkühler, 2002), neurons were classified based on repetitive firing behavior including tonic firing, phasic firing, delayed firing or depolarizing block.

2.10 Flow cytometry

To sort astrocytes and neurons, cells were isolated as previously described (Nguyen et al., 2020). The spinal lumbar enlargements of mice were minced and then digested using an Adult Brain Dissociation Kit (Miltenyi Biotec, Shanghai, China) and gentleMACS Octo Dissociator with Heaters (Miltenyi Biotec, Shanghai, China). After tissue digestion, cells were filtered through a 70-μm pore cell-strainer to obtain a single-cell suspension. Then the myelin, debris and red blood cells were removed from the single-cell suspension. To fix and permeabilize cells, the single-cell suspension was resuspended in an eBioscience™ FOXP3/ Transcription Factor Staining Buffer Set (Invitrogen). For sorting astrocytes and neurons, we used the following fluorochrome-coupled antibodies: RBFOX3/NeuN (IB7) [PE] (NOVUS, Medtronic, MN, USA), GFAP Monoclonal Antibody, Alexa Fluor 647 (Invitrogen, Carlsbad, CA, USA), eBioscience™ Fixable Viability Dye eFluor 780 (Invitrogen, Carlsbad, CA, USA). Cells were sorted on a FACSAria SORP Flow Cytometer (BD Biosciences, San Jose, CA, USA).

2.11 Single-cell RNA sequencing (scRNA-seq) and analysis

The single-cell suspension of the spinal lumbar enlargement was obtained in the same way as described for flow cytometry (*vide supra*). The cells were filtered through a 40-μm pore cell-strainer. The single-cell suspension was loaded into Chromium microfluidic chips with 30 chemistry and barcoded with a 10 Chromium Controller (10X Genomics). RNA from the barcoded cells was subsequently reverse-transcribed and sequencing libraries were constructed with reagents from a Chromium Single Cell 30 reagent kit (10X Genomics) according to the manufacturer's instructions. Sequencing was performed with an Illumina NovaSeq 6000 according to the manufacturer's instructions (Illumina).

Raw reads were demultiplexed and mapped to the reference genome by a 10X Genomics Cell Ranger pipeline using the default parameters. All downstream single-cell analyses were performed using Cell Ranger and Seurat (Macosko et al., 2015), unless mentioned specifically. In brief, for each gene and each cell barcode (filtered by Cell Ranger), unique molecule identifiers were counted to construct digital expression matrices. Secondary filtration by Seurat: A gene with expression detected in more than 3 cells was considered to be expressed, and each cell was required to have at least 200 expressed genes. Contaminating cells were filtered to obtain an enriched population of the cell type of interest.

GO enrichment analysis of marker genes was implemented using the cluster Profiler R package, in which gene length bias was corrected. GO terms with corrected *P*-values < 0.05 were considered to be significantly enriched by a marker gene. The cluster Profiler R package was used to test for the statistical enrichment of marker genes in KEGG pathways (http://www.genome.jp/kegg/) (Kanehisa & Goto, 2000).

2.12 Statistical analysis

Data were given as mean ± SD and statistical analyses were performed using GraphPad Prism 8.0 software (GraphPad Software, CA, USA). All data from different groups were verified for normality and homogeneity of variance using Kolmogorov Smirnov and Brown

Forsythe tests before analysis. Data were compared using paired or unpaired Student's *t*-tests or a Wilcoxon test as appropriate. The time courses of behavioral results were analyzed using a two-way repeated measures analysis of variance (ANOVA) followed by a Bonferroni post hoc test. Cochran–Armitage trend test was used to compare the trends between two groups. The exact analysis used for each comparison is described in each figure legend. A P-value < 0.05 was considered to be statistically significant.

3. Results

3.1 Reduced expression of Kir4.1 contributes to CCI-induced hyperalgesia

To confirm that Kir4.1 is preferentially expressed by spinal cord astrocytes, we characterized Kcnj10 transcript expression in spinal lumbar enlargement samples from human (GSE189501) (D. Zhang et al., 2022) and mouse (GSE103892) (Sathyamurthy et al., 2018) publicly available transcriptomic databases. As expected, Kcnj10 transcript is widely expressed in spinal cord glial cells, including oligodendrocytes and astrocytes, but minimal levels were detected in neurons (Fig. S1A, S1B).

Next, we wanted to determine whether cell-type-specific expression of Kir4.1 is altered in a CCI-induced mouse model of neuropathic pain. All the mice tested developed hyperalgesia one day after CCI, and the pain lasted for at least 2 weeks (n = 20, male = 10, female = 10, Figs. 1A, 1B). Consistent with evidence that peripheral nerve injury induces spinal astrocyte proliferation (Cirillo et al., 2015), we found that the expression of GFAP was increased in the CCI-ipsi side of the spinal lumbar enlargement (compared to the CCI-contra side) at day 7 (n = 6, male = 3, female = 3, $P = 0.037$) and day 14 (n = 6, male = 3, female = 3, $P = 0.005$) (Fig. S2). Immunofluorescence staining of Kir4.1 and GFAP was performed on spinal lumbar enlargement samples on day 1 and day 14 after CCI. The images, shown in Figs. 1D and 1H, indicated that Kir4.1 was expressed in astrocytes; the quantitative data for Kir4.1 obtained by RT-PCR and Western blot analysis were shown in Figs. 1C, 1E–G. Consistent with evidence that nerve injury negatively impacts expression of Kir4.1 (Vit et al., 2008), we found Kir4.1 transcript and protein levels to be decreased on the ipsilateral side 7 and 14 days after CCI (Figs. 1F, 1G). Conversely, the expression of Kir4.1 transcript and protein remained similar to control at days 1 (Fig. 1C) and 3 (Fig. 1E) in the ipsilateral lumbar enlargement (compared to the CCI-contra side). Additionally, we obtained enriched populations of astrocytes from the spinal lumbar enlargements (Fig. 1I) and confirmed that Kir4.1 transcript was decreased in ipsilateral astrocytes compared to contralateral astrocytes on day 14 after CCI (1.03 ± 0.27 *vs.* 0.45 ± 0.17, n = 5, $P = 0.004$, Fig. 1J).

3.2 CCI-induced changes in astrocyte gene expression

We used a nonbiased single-cell transcriptomic approach to identify CCI-sensitive genes in spinal astrocytes. RNA sequencing was performed on samples collected 14 days after CCI (Fig. 2A). The accession number for both the raw sequencing data and the processed data reported in this paper is GEO: GSE208766. We obtained 27,188 individual cells (13,538 from the CCI-contra side, 13,650 from the CCI-ipsi side) from the spinal lumbar enlargements of 8 mice (8 weeks old). Cells were classified into 10 cell types (Fig. 2B) with distinct gene expression profiles (Figs. 2D–F). The sensitivity of astrocytes to nerve injury

was evidenced by the multitude of genes affected in these cells after CCI. CCI-sensitive genes in astrocytes included Kir4.1 (*Kcnj10*), MeCP2 and TWIK-1 (*Kcnk6*), the latter a leak K^+ channel known to contribute to astrocyte membrane potential, sodium channels (e.g., Scn1a, Scn3a, NALCN) and purinergic receptors (e.g., P2rx7, P2ry2, P2ry12). Of these, expression of both Kir4.1 and MeCP2 was diminished in astrocytes following CCI (Fig. 2H). These results further suggest that reduced expression of MeCP2 and Kir4.1 contributes to hyperalgesia in CCI. We also performed gene ontology (GO) term analysis to explore functional properties of enriched genes in all cells, astrocytes and microglia on day 7 (Figs. S3H–J) and day 14 (Fig. S4) after CCI. Enriched genes on day 7 after CCI were mainly associated with neurodegeneration (Figs. S3H, S3I–J). Of note, on day 14 after CCI, microglia also showed increased expression of genes associated with activation/pro-inflammation (Fig. S5).

To better determine whether CCI results in cell-type-specific changes in Kir4.1 expression, we characterized Kcnj10 expression in various cell types, comparing the CCI-ipsi side with the CCI-contra side of spinal lumbar enlargements. We found that 14 days after CCI, expression of Kcnj10 in astrocytes on the CCI-ipsi side of the spinal lumbar enlargement significantly decreased relative to astrocytes on the opposite side. Kcnj10 transcript was unchanged in other cell types (Fig. S1C). These results suggest that expression of Kir4.1 was diminished in ipsilateral astrocytes one weeks after CCI in the spinal cord.

3.3. Conditional knockdown expression of Kir4.1 in spinal astrocytes induces hyperalgesia

To determine whether reduced expression of astrocytic Kir4.1 channels contributes to hyperalgesia, we generated astrocyte-specific inducible Kir4.1 cKO by crossing $GFAP^{Cre\text{-}ERT2}$ mice with $Kir4.1^{f/f}$ mice (Fig. 3A). We confirmed by immunohistochemistry that Kir4.1 was diminished in astrocytes from Kir4.1 cKO compared to the control (Fig. 3B; the white color was reduced). We also confirmed at the transcript level by PCR that Kir4.1 mRNA was decreased by 39.0% ± 16.1% (n = 6, male = 3, female = 3, P = 0.004, Fig. 3C) in the spinal lumbar enlargement of Kir4.1 cKO mice. Consistent with our hypothesis, Kir4.1 cKO mice were highly sensitive to mechanical ($P < 0.001$, Fig. 3D) and thermal ($P < 0.001$, Fig. 3E) sensations (n =10, male = 5, female = 5). To investigate more specifically the roles of Kir4.1 channels in spinal astrocytes, we injected 5 μL AAV2/8-gfaABC1D-eGFP-P2A-iCre-WPRE-pA (AAV-GFAP-iCRE) into the spinal lumbar enlargement of $Kir4.1^{f/f}$ mice (Fig. 3F) to knockdown astrocytic Kir4.1 expression in a region-specific manner. We confirmed the specificity of Cre-recombinase expression immunohistochemically; tissue isolated 4 weeks after viral injection showed that GFP^+-transfected cells were GFAP-immunoreactive astrocytes (Fig. 3G). We also confirmed that 6 weeks after intrathecal injection, Kir4.1 knockdown mice showed a 24.0% ± 12.6% reduction in Kir4.1 mRNA compared to mice that received control virus (n = 7, male = 3, female = 4, P = 0.017, Fig. 3L). To further validate knockdown of our target transcript, we isolated enriched populations of astrocytes from mice injected with AAV-GFAP-iCRE or control virus (Fig. 3H). We found that Kir4.1 knockdown mice showed a 66.7% ± 20.9% decrease in Kir4.1 transcript compared to astrocytes from control animals (n = 5, male = 3, female = 2, $P < 0.001$, Fig. 3I). Consistent with global Kir4.1 cKO mice, we found that

Kir4.1 knockdown mice also exhibited hyperalgesia in response to mechanical (n = 10, male = 5, female = 5, $P < 0.001$, Fig. 3J) and thermal (n = 10, male = 5, female = 5, $P < 0.001$, Fig. 3K) stimulation.

3.4 Overexpression of Kir4.1 relieves hyperalgesia behaviors in Kir4.1 cKO mice and CCI mice

Next, we wanted to determine whether overexpression of Kir4.1 ameliorates hyperalgesia in both Kir4.1 cKO mice and a mouse model of neuropathic pain. We injected AAV2/8-hEF1a-DIO-kcnj10–2A-eGFP-WPRE-pA (AAV-Kir4.1) into the spinal cord of Kir4.1 cKO mice to drive expression of Kir4.1 (*Kcnj10*) specifically in astrocytes (Fig. 4A). We confirmed that this approach increased Kir4.1 mRNA levels in the spinal lumbar enlargement of Kir4.1 cKO mice by 47.2% ± 19.0% (n = 6, male = 3, female = 3, $P = 0.003$, Fig. 4B). Behaviorally, we found that re-expression of Kir4.1 decreased the sensitivity of mice to both mechanical (n = 6, male = 3, female = 3, $P < 0.001$, Fig. 4C) and thermal (n = 6, male = 3, female = 3, $P = 0.004$, Fig. 4D) stimuli compared to Kir4.1 cKO mice injected with control virus. It should be noted that re-expression of Kir4.1 did not produce analgesic effects compared to $Kir4.1^{f/f}$ mice (Fig. S6).

As re-expression of Kir4.1 ameliorated the behavioral hyperalgesia induced by Kir4.1 cKO, we wondered whether overexpression of Kir4.1 might show promise as a treatment for hyperalgesia in neuropathic pain. To test whether Kir4.1 might play a therapeutic role in neuropathic pain, we injected AAV-Kir4.1 and AAV2/8-gfaABC1D-iCre-WPRE-pA (AAV-iCRE) (2.5 μL; injected in equal proportions) into the spinal cord 7 days after CCI (Fig. 4H). This approach increased Kir4.1 mRNA in spinal lumbar enlargement astrocytes from wild-type mice by 69.5% ± 13.7% (n = 5, male = 2, female = 3, $P = 0.009$, Fig. 4E, 4F). We confirmed the specificity of AAV expression by immunofluorescence, finding that GFP^+ transfected cells were well merged with GFAP-immunoreactive astrocytes (Fig. 4G). We also confirmed that 4 weeks after intrathecal injection, Kir4.1 overexpression in CCI mice showed a 20.5% ± 10.5% increase in Kir4.1 mRNA compared to mice that received control virus (n = 8, male = 4, female = 4, $P = 0.009$, Fig. 4K). Importantly, we found that CCI-induced hyperalgesia for mechanical (n = 7, male = 4, female = 3, $P < 0.001$, Fig. 4I) and thermal sensations (n = 7, male = 4, female = 3, $P < 0.001$, Fig. 4J) was eliminated by overexpression of Kir4.1. These results identify astrocytic Kir4.1 channels as a high-priority therapeutic target for neuropathic pain.

3.5 Knockdown of Kir4.1 disrupts neuronal firing patterns in the dorsal spinal cord

In other brain regions, diminished Kir4.1 expression has been shown to disrupt neural firing behavior in favor of increased tonic activity(Cui et al., 2018); therefore, we wondered whether a similar phenomenon occurs at the level of the spinal cord. To test this, Kir4.1-siRNA (5’-ACAAAGGAGGGTGAGAATATT-3’) or control-siRNA was injected intrathecally into neonatal wild-type mice (P12) to knockdown Kir4.1 expression in the spinal cord (Fig. 5A). Immunofluorescence staining was performed on the spinal cord 2 days after injection (Fig. 5B). Kir4.1 mRNA was decreased by 51.6% ± 20.2% in the spinal cord after injection of Kir4.1-siRNA (n = 5, $P = 0.002$, Fig. 5C). To assess Kir4.1 function in spinal astrocytes, we made whole-cell current- and voltage-clamp recordings

from astrocytes in spinal lumbar enlargement slices 2–4 days after Kir4.1-siRNA injection (Fig. 5D). Consistent with a requisite role of Kir4.1 in setting astrocyte resting membrane potential (RMP) (Nwaobi, Cuddapah, Patterson, Randolph, & Olsen, 2016), we found that astrocytes in slices from Kir4.1-siRNA mice were depolarized compared to astrocytes from control-siRNA mice (−81.55 ± 0.31 mV *vs.* −77.53 ± 3.48 mV, $P = 0.029$, Fig. 5E). Also, in voltage-clamp (Vhold −80 mV; in TTX to block neural action potentials), astrocytes in slices from Kir4.1-siRNA mice showed less outward current (102.40 ± 58.42 pA *vs.* 37.33 ± 24.58 pA, $P = 0.007$) at a holding potential of −80 mV (Fig. 5F) and a smaller change in conductance in response to 50 mV steps (12.25 ± 7.25 nS *vs.* 4.30 ± 2.04 nS, $P = 0.006$) compared to control mice (Fig. 5I). To gauge contributions of Kir channels to astrocyte electrical properties in each genotype, in voltage clamp mode ($V_{holding} = -80$ mV), we measured holding current and conductance (in response to 50 mV steps every 170 ms) during exposure to Ba^{2+}, a pan-Kir channel blocker. Bath application of $BaCl_2$ (100 μM) decreased the holding current and conductance by 103.02 ± 49.12 pA and 7.54 ± 3.30 nS, respectively, in control astrocytes (Fig. 5H, left). Conversely, astrocytes from Kir4.1-siRNA mice showed only a modest Ba^{2+}-induced change in holding current (33.30 ± 16.41 pA, $P = 0.002$) and conductance (2.33 ± 1.02 nS, $P < 0.001$) (Fig. 5H, right; Fig. 5J). Further, the Ba^{2+}-sensitive current in astrocytes from both genotypes reversed at −96 mV and showed a modest degree of inward rectification at potentials positive to −20 mV (Fig. 5G). These results provide functional conformation of diminished Kir4.1 channel function in astrocytes from Kir4.1-siRNA mice.

To investigate how reduced expression of astrocytic Kir4.1 transcript impacts neural activity, we made whole-cell current-clamp recordings from neurons in spinal lamina I and II (Fig. 5K). We found that neurons in slices from Kir4.1-siRNA mice were depolarized compared to neurons from control tissue ($P = 0.019$, Fig. 5L). We also found that spinal lamina I and II neurons can be subclassified based on distinguishing their repetitive firing behavior, including tonic firing, phasic firing, delayed firing or depolarizing block (Fig. 5N). Interestingly, the proportion of tonic firing neurons was increased in slices from Kir4.1-siRNA-treated mice (Figs. 5O–T). For example, under baseline conditions (0-pA injection), the proportion of tonic firing neurons increased to 23% in slices from Kir4.1-siRNA-treated mice, compared to only 5% in control neurons (Fig. 5O). When response to moderate currents injection, a 30-pA and/or 60-pA current injection elicited tonic firing in 70% and/or 50% of control neurons and respectively increased to 77% and/or 69% of neurons in slices from Kir4.1-siRNA mice (Figs. 5P, 5Q). However, in response to larger current injections (e.g., 90-pA step), neurons from both genotypes showed pronounced decrements in action potential amplitude and frequency, indicative of depolarizing block; consequently the proportion of tonic firing neurons in slices from control and Kir4.1-siRNA mice fell to 35% and 23%, respectively (Fig. 5R). These results suggest that neurons in Kir4.1siRNA-treated mice were better able to maintain tonic firing in response to spontaneous conditions and/or moderate stimulation compared to neurons from control-siRNA-treated mice ($P < 0.001$, Fig. 5T), which is consistent with the hyperalgesia response elicited by moderate stimulation *in vivo*. Of note, astrocyte-specific knockdown of Kir4.1 did not affect neural input resistance ($P = 0.997$, Fig. 5M), but it decreased AP amplitude ($P = 0.033$, Fig. S7A)

and increased AP width ($P = 0.048$, Fig. S7B), which are consistent with dysregulation of extracellular K^+.

3.6 Knockdown of MeCP2 in astrocytes induces hyperalgesia

Based on evidence that MeCP2 regulates expression of Kir4.1 in astrocytes (Kahanovitch et al., 2018), we wondered if chronic pain decreases MeCP2 levels and whether hyperalgesia in MeCP2-deficient mice could be rescued by the expression of Kir4.1 in spinal astrocytes. Neuropathic pain was induced by CCI in mice. All mice tested developed hyperalgesia by 1 day after CCI that lasted for at least 2 weeks (n = 12, male = 6, female = 6; Figs. 6A–B). Consistent with evidence from a spared nerve injury mouse model of chronic pain (Tochiki et al., 2012), we found that expression of MeCP2 in the spinal lumbar enlargement decreased on the ipsilateral side (as compared to the contralateral side) by day 3 following CCI (Fig. 6E) and remained low for up to 2 weeks after CCI (Figs. 6F–G). At day 1, the expression levels of MeCP2 transcript and protein remained similar to control levels (Fig. 6C). Immunofluorescence staining performed on spinal lumbar enlargement on day 1 and day 14 after CCI show detectable levels of MeCP2 in both neurons and astrocytes (Figs. 6D and 6H). Unexpectedly, the expression of MeCP2 in astrocytes was preferentially disrupted in this model. FACS-enriched populations of neurons and astrocytes from the ipsilateral spinal lumbar enlargement 14 days after CCI (Fig. 6I) show that MeCP2 transcript was decreased in astrocytes (1.04 ± 0.31 *vs.* 0.47 ± 0.16, n = 5, male = 2, female = 3, $P = 0.007$; Fig 6K) but unchanged in neurons (1.00 ± 0.09 *vs.* 0.92 ± 0.22, n = 5, male = 2, female = 3, $P = 0.471$; Fig 6J). These results suggest that expression of MeCP2 is preferentially diminished in ipsilateral astrocytes 14 days after CCI in the spinal cord.

To functionally differentiate neuron and astrocyte roles of MeCP2 in pain sensitivity, we used hSyn and gfaABC1D promoter-driven RNA interference to knockdown MeCP2 levels in spinal cord neurons (AAV2/8-hSyn-miRNAi(mecp2)-eGFP-WPRE-pA: AAV-hSyn-RNA) or astrocytes (AAV2/8-gfaABC1D-miRNAi(mecp2)-mCherry-WPRE-pA: AAV-GFAP-RNA) (Figs. 7A, 7J). Four weeks after viral injection, we characterized cell-type-specific expression of MeCP2 and behavioral responses to mechanical and thermal pain. The specificity of our approach was confirmed immunohistochemically using antibodies to NeuN (Fig. 7B) and GFAP (Fig. 7K). To confirm the cell specificity of this approach, we also characterized MeCP2 transcript levels in FACS-enriched populations of neurons or astrocytes obtained from wild-type mice injected with AAV-hSyn-RNA (Fig. 7C). Consistent with expectations, MeCP2 transcript levels were decreased in neurons (1.06 ± 0.40 vs. 0.44 ± 0.12, n = 5, male = 3, female = 2, $P = 0.011$, Fig. 7D) but not in astrocytes ($P = 0.679$, Fig. 7E). In parallel, we also obtained FACS-enriched populations of neurons or astrocytes from AAV-GFAP-RNA-injected wild-type mice (Fig. 7L) and confirmed that MeCP2 levels were decreased in astrocytes (1.05 ± 0.37 vs. 0.58 ± 0.16, n = 5, male = 3, female = 2, $P = 0.031$, Fig. 7N) but not in neurons ($P = 0.835$, Fig. 7M). At the behavioral level, we found that astrocyte-specific MeCP2 knockdown produced hyperalgesia (Figs. 7O, 7P), whereas neuron-specific MeCP2 knockdown mice responded to mechanical and thermal stimuli in a manner similar to control mice (Figs. 7F, 7G). We also confirmed that 5 weeks after intrathecal injection, neuron-specific MeCP2 knockdown mice showed a 30.5% ± 10.6% reduction in MeCP2 mRNA compared to mice that received control virus (n =

10, male = 5, female = 5, $P < 0.001$, Fig. 7H), and astrocyte-specific MeCP2 knockdown caused a 18.1% ± 9.6% reduction (n = 10, male = 5, female = 5, $P = 0.003$, Fig. 7Q). Consistent with evidence that MeCP2 regulates expression of astrocytic Kir4.1 channels (Kahanovitch et al., 2018), we found that AAV-GFAP-RNA-injected wild-type mice showed reduced Kir4.1 expression in astrocytes (23.7% ± 10.4%, n = 10, male = 5, female = 5, $P = 0.001$, Fig.7R), whereas the neural levels of Kir4.1 were similar to those of control mice (n = 10, male = 5, female = 5, $P = 0.497$, Fig. 7I). These results suggest that reduced expression of astrocytic Kir4.1 channels contributes to pain sensitivity in MeCP2-deficient mice.

3.7 Overexpression of MeCP2 in astrocytes increases Kir4.1 expression and ameliorates hyperalgesia in a CCI mouse model of neuropathic pain

If reduced expression of MeCP2 and Kir4.1 causes neuropathic pain in CCI, then over-expression of MeCP2 is expected to minimize pain sensitivity in this model. To test this hypothesis, we performed intrathecal injections of AAV2/8-pTight-eGFP-WPRE-pA and AAV2/8-gfaABC1D-rtTAV16-WPRE-pA (AAV-GFAP-MeCP2, 2.5 μL, injected in equal proportions) and, 4 weeks later, administered doxycycline (Dox) orally to drive expression of MeCP2 in CCI-treated wild-type mice (Fig. 8A). We confirmed the specificity of AAV expression by immunofluorescence that GFP^+ transfected cells were well merged with GFAP-immunoreactive astrocytes (Fig. 8B). We further validated this approach by obtaining FACS-enriched populations of neurons or astrocytes from wild-type mice 5 weeks after injection of AAV-GFAPMeCP2 and 1 week following administration of Dox (Fig. 8C). We confirmed that MeCP2 transcript was selectively increased in astrocytes (1.01 ± 0.16 *vs.* 1.48 ± 0.29, n = 5, male = 3, female = 2, $P = 0.013$; Fig. 8E), but not in neurons (1.12 ± 0.59 *vs.* 1.22 ± 0.50, n = 5, male = 3, female = 2, $P = 0.791$; Fig. 8D). At the functional level, we found that over-expression of MeCP2 in astrocytes prevented CCI-induced hyperalgesia (Figs. 8F, 8G). We also confirmed expression of MeCP2 was increased by 22.0% ± 8.9% (n = 6, male = 3, female = 3, $P = 0.007$, Fig. 8H) on day 14 after CCI, and this occurred in conjunction with increased expression of Kir4.1 (by 46.0% ± 10.5%, n = 6, male = 3, female = 3, $P = 0.006$, Fig. 8I). Of note, there was no change of MeCP2 expression in Kir4.1 cKO mice (Fig. S8A, related to Fig. 3C), AAV-GFAP-iCRE-injected $Kir4.1^{f/f}$ mice (Fig. S8B, related to Fig. 3L), or AAV-Kir4.1 overexpression mice (Fig. S8C, related to Fig. 4B; Fig. S8D, related to Fig. 4K), thus suggesting MeCP2 expression in astrocytes was not voltage dependent. Together, these results identify reduced expression of MeCP2 and Kir4.1 channels in spinal astrocytes as the basis for hyperalgesia in CCI.

4. Discussion

Cellular and molecular mechanisms contributing to chronic neuropathic pain are not well understood and treatment options are limited. Here, we identify MeCP2 and Kir4.1 channels in spinal astrocytes as both necessary and sufficient for hyperalgesia in two mouse models of chronic pain. Surprisingly, peripheral nerve injury preferentially disrupted expression of MeCP2 in spinal astrocytes but not in neurons, and this coincided with loss of Kir4.1 function and increased sensitivity to thermal and mechanical sensation. This hyperalgesia phenotype was mimicked by astrocyte-specific Kir4.1 knockdown and ameliorated by re-

expression of Kir4.1 or MeCP2 in spinal astrocytes. These results highlight astrocytic Kir4.1 channels as a promising target for treatment of chronic neuropathic pain.

A likely mechanism by which reduced expression of Kir4.1 augments pain transduction involves dysregulation of extracellular K^+. For example, astrocytic Kir4.1 channels serve as a main conduit for K^+ uptake from the extracellular space during high neural activity, and disruption of this process is expected to amplify pain transduction. In other brain regions, genetic ablation (Cui et al., 2018) or pharmacological inhibition (Ohno, Kinboshi, & Shimizu, 2018) of Kir4.1 has been shown to increase extracellular K^+ during stimulated neural activity, and there is a wealth of evidence that high extracellular K^+ can increase neural activity (Brocard et al., 2013; Wang et al., 2012). Elevated or decreased extracellular K^+ has long been known to modulate neuronal activity (Brocard et al., 2013), firing pattern (Cui et al., 2018) and synaptic neurotransmitter release (Rimmele, Rocher, Wellbourne-Wood, & Chatton, 2017), which may contribute to pain processing in dorsal spinal cord. Consistent with this, we showed that knockdown of Kir4.1 increased the tonic firing behavior of spinal neurons in response to modest stimuli and tended to cause depolarizing block at very high frequencies. These results suggest diminished astrocyte Kir4.1 expression results in high extracellular K^+ and favors increased neural activity. However, the opposite is not necessarily the case; increased expression of Kir4.1 does not have an analgesic effect, presumably because the ability of astrocytes to lower extracellular K^+ below normal levels is limited by the K^+ reversal potential (floor effect). Therefore, reduced expression of astrocytic Kir4.1 channels can enhance the ability of pain relay neurons to maintain stimulated activity, which conceivably contributes to hyperalgesia *in vivo*. This is also consistent with recent evidence that the membrane dynamics of astrocytes may drive neuronal activity in circuit-specific ways (Armbruster et al., 2022). Gliosis that often accompanies reduced expression of Kir4.1 following CCI is expected to decrease extracellular volume, and thus further increase the impact of extracellular K^+ on neural activity.

Kir4.1 channels are also important determinants of astrocyte membrane potential (Olsen, Higashimori, Campbell, Hablitz, & Sontheimer, 2006), and consequently regulate various voltage-dependent processes, including glucose uptake, activity of the sodium calcium exchanger (NCX) and release of neuromodulators. Consistent with this, previous studies showed that astrocyte-specific loss of Kir4.1 function depolarized astrocyte membrane potential and decreased glutamate uptake (Djukic, Casper, Philpot, Chin, & McCarthy, 2007). Astrocyte depolarization will also favor Ca^{2+} influx via reverse mode operation of the NCX to promote release of adenosine triphosphate (ATP) and cytokines (Rose, Ziemens, & Verkhratsky, 2020; Sobrinho, Gonçalves, Takakura, Mulkey, & Moreira, 2017). Accordingly, previous studies showed that astrocytes release ATP following peripheral nerve injury and this activates purinergic receptors on spinal neurons, leading to increased neuronal excitability and hyperalgesia (Illes, Khan, & Rubini, 2017; Koyanagi et al., 2016; X. Zhang & Li, 2019).

In recent years, several studies have implied a role for MeCP2 in pain processing (Manners, Tian, Zhou, & Ajit, 2015; Tajerian et al., 2013; Tochiki et al., 2012; R. Zhang et al., 2015). For example, i) patients with Rett syndrome (caused by mutation of MeCP2) report

abnormal sensory function (Barney, Feyma, Beisang, & Symons, 2015; Downs et al., 2010); ii) MeCP2 knockout rats show hypersensitivity to mechanical stimulation (Bhattacherjee et al., 2017) and iii) overexpression of MeCP2 reduced mechanical and thermal pain sensitivity, suggesting an analgesic role of MeCP2 in pain transduction (R. Zhang et al., 2015). Previous work also showed that the expression of MeCP2 was reduced in a cell-type-specific manner following nerve injury (Orefice et al., 2016; Tochiki et al., 2012). Here, we extended these findings by showing that the expression of MeCP2 in spinal astrocytes is selectively disrupted following nerve injury. Further, since MeCP2 regulates expression of Kir4.1 channels by binding to Kcnj10 promoters (Kahanovitch et al., 2018), we reasoned that reduced expression of MeCP2 and Kir4.1 in spinal astrocytes contributes to the development of chronic neuropathic pain. This possibility is supported by evidence that overexpression of Kir4.1 in spinal astrocytes alleviated hyperalgesia in both CCI and spinal MeCP2-deficient mice, highlighting Kir4.1 as an underlying therapeutic target for the sensory abnormality in Rett syndrome. However, it should be recognized that MeCP2 is ubiquitously expressed and hyperalgesia associated with loss of this transcription factor is likely multifactorial involving multiple cell types.

For example, although we showed that reduced expression of MeCP2 from spinal neurons has a negligible effect on pain sensitivity, others have shown that deletion of MeCP2 from peripheral sensory neurons resulted in hypersensitivity to touch by a mechanism involving loss of GABA receptors on sensory neuron terminals and subsequent loss of presynaptic inhibition (Orefice et al., 2016). Dysregulation of inhibitory signaling by astrocytes has also been shown to contribute to hyperalgesia in other pain models (Ng & Ong, 2001). Therefore, it is likely that peripheral sensory-neuron-specific loss of MeCP2 increases neural excitability directly, whereas pathological changes in spinal astrocytes promote hyperexcitability of pain processing (Ji, Donnelly, & Nedergaard, 2019; Xu et al., 2021).

In summary, reduced expression of MeCP2 following nerve injury results in reduced expression of astrocytic Kir4.1 channels, which contributes to hyperalgesia in the chronic phase of neuropathic pain. Therefore, targeting Kir4.1 may be a novel treatment approach for chronic pain after nerve injury.

Supplementary Material

Refer to Web version on PubMed Central for supplementary material.

Acknowledgments

We thank Huifang Li, from the Core Facilities of West China Hospital, Sichuan University, for her help in FACS. We also thank Dr. Wenxing Yang, from the Department of Physiology, West China School of Preclinical and Forensic Medicine, for his advice in electrophysiology analysis; and Dr. Benjamin Gelman from Department of Pathology, University of Texas Medical Branch for providing human spinal lysates.

Funding

This work was supported by the grant No. 2018YFC2001800/2018YFC2001804-1 (M.O.), No. 2020YFC2008402 (C.Z.) from National Key Research and Development Program of China; grant No. 82001183 (M.O.) from the National Natural Science Foundation of China; 21PJ013 (Y.C.) from the Health Commission of Sichuan province program of China; and NIH grants R01NS079166 (S.J.T.), R01DA050530 (S.J.T.).

References

Armbruster M, Naskar S, Garcia JP, Sommer M, Kim E, Adam Y, . . . Dulla CG. (2022). Neuronal activity drives pathway-specific depolarization of peripheral astrocyte processes. Nat Neurosci, 25(5), 607–616. doi:10.1038/s41593-022-01049-x [PubMed: 35484406]

Ballas N, Lioy DT, Grunseich C, & Mandel G. (2009). Non-cell autonomous influence of MeCP2-deficient glia on neuronal dendritic morphology. Nat Neurosci, 12(3), 311–317. doi:10.1038/nn.2275 [PubMed: 19234456]

Barney CC, Feyma T, Beisang A, & Symons FJ (2015). Pain experience and expression in Rett syndrome: Subjective and objective measurement approaches. J Dev Phys Disabil, 27(4), 417–429. doi:10.1007/s10882-015-9427-3 [PubMed: 26425056]

Bennett GJ, & Xie YK (1988). A peripheral mononeuropathy in rat that produces disorders of pain sensation like those seen in man. Pain, 33(1), 87–107. doi:10.1016/0304-3959(88)90209-6 [PubMed: 2837713]

Bhattacherjee A, Mu Y, Winter MK, Knapp JR, Eggimann LS, Gunewardena SS, . . . Smith PG. (2017). Neuronal cytoskeletal gene dysregulation and mechanical hypersensitivity in a rat model of Rett syndrome. Proc Natl Acad Sci U S A, 114(33), E6952–e6961. doi:10.1073/pnas.1618210114 [PubMed: 28760966]

Brocard F, Shevtsova NA, Bouhadfane M, Tazerart S, Heinemann U, Rybak IA, & Vinay L. (2013). Activity-dependent changes in extracellular Ca2+ and K+ reveal pacemakers in the spinal locomotor-related network. Neuron, 77(6), 1047–1054. doi:10.1016/j.neuron.2013.01.026 [PubMed: 23522041]

Chang Q, Khare G, Dani V, Nelson S, & Jaenisch R. (2006). The disease progression of Mecp2 mutant mice is affected by the level of BDNF expression. Neuron, 49(3), 341–348. doi:10.1016/j.neuron.2005.12.027 [PubMed: 16446138]

Cirillo G, Colangelo AM, Berbenni M, Ippolito VM, De Luca C, Verdesca F, . . . Papa M. (2015). Purinergic Modulation of Spinal Neuroglial Maladaptive Plasticity Following Peripheral Nerve Injury. Mol Neurobiol, 52(3), 1440–1457. doi:10.1007/s12035-014-8943-y [PubMed: 25352445]

Cohen SP, & Mao J. (2014). Neuropathic pain: mechanisms and their clinical implications. Bmj, 348, f7656. doi:10.1136/bmj.f7656 [PubMed: 24500412]

Colloca L, Ludman T, Bouhassira D, Baron R, Dickenson AH, Yarnitsky D, . . . Raja SN. (2017). Neuropathic pain. Nat Rev Dis Primers, 3, 17002. doi:10.1038/nrdp.2017.2 [PubMed: 28205574]

Cui Y, Yang Y, Ni Z, Dong Y, Cai G, Foncelle A, . . . Hu H. (2018). Astroglial Kir4.1 in the lateral habenula drives neuronal bursts in depression. Nature, 554(7692), 323–327. doi:10.1038/nature25752 [PubMed: 29446379]

Dixon WJ (1991). Staircase bioassay: the up-and-down method. Neurosci Biobehav Rev, 15(1), 47–50. doi:10.1016/s0149-7634(05)80090-9 [PubMed: 2052197]

Djukic B, Casper KB, Philpot BD, Chin LS, & McCarthy KD (2007). Conditional knock-out of Kir4.1 leads to glial membrane depolarization, inhibition of potassium and glutamate uptake, and enhanced short-term synaptic potentiation. J Neurosci, 27(42), 11354–11365. doi:10.1523/jneurosci.0723-07.2007 [PubMed: 17942730]

Downs J, Géranton SM, Bebbington A, Jacoby P, Bahi-Buisson N, Ravine D, & Leonard H. (2010). Linking MECP2 and pain sensitivity: the example of Rett syndrome. Am J Med Genet A, 152a(5), 1197–1205. doi:10.1002/ajmg.a.33314 [PubMed: 20425824]

Finnerup NB, Kuner R, & Jensen TS (2021). Neuropathic Pain: From Mechanisms to Treatment. Physiol Rev, 101(1), 259–301. doi:10.1152/physrev.00045.2019 [PubMed: 32584191]

Fukuda T, Itoh M, Ichikawa T, Washiyama K, & Goto Y. (2005). Delayed maturation of neuronal architecture and synaptogenesis in cerebral cortex of Mecp2-deficient mice. J Neuropathol Exp Neurol, 64(6), 537–544. doi:10.1093/jnen/64.6.537 [PubMed: 15977646]

Gao YJ, & Ji RR (2010). Targeting astrocyte signaling for chronic pain. Neurotherapeutics, 7(4), 482–493. doi:10.1016/j.nurt.2010.05.016 [PubMed: 20880510]

Gaskin DJ, & Richard P. (2012). The economic costs of pain in the United States. J Pain, 13(8), 715–724. doi:10.1016/j.jpain.2012.03.009 [PubMed: 22607834]

Géranton SM, Fratto V, Tochiki KK, & Hunt SP (2008). Descending serotonergic controls regulate inflammation-induced mechanical sensitivity and methyl-CpG-binding protein 2 phosphorylation in the rat superficial dorsal horn. Mol Pain, 4, 35. doi:10.1186/1744-8069-4-35 [PubMed: 18793388]

Géranton SM, Morenilla-Palao C, & Hunt SP (2007). A role for transcriptional repressor methyl-CpG-binding protein 2 and plasticity-related gene serum- and glucocorticoid-inducible kinase 1 in the induction of inflammatory pain states. J Neurosci, 27(23), 6163–6173. doi:10.1523/jneurosci.1306-07.2007 [PubMed: 17553988]

Goldberg DS, & McGee SJ (2011). Pain as a global public health priority. BMC Public Health, 11, 770. doi:10.1186/1471-2458-11-770 [PubMed: 21978149]

Hargreaves K, Dubner R, Brown F, Flores C, & Joris J. (1988). A new and sensitive method for measuring thermal nociception in cutaneous hyperalgesia. Pain, 32(1), 77–88. doi:10.1016/0304-3959(88)90026-7 [PubMed: 3340425]

Illes P, Khan TM, & Rubini P. (2017). Neuronal P2X7 Receptors Revisited: Do They Really Exist? J Neurosci, 37(30), 7049–7062. doi:10.1523/jneurosci.3103-16.2017 [PubMed: 28747388]

Ji RR, Donnelly CR, & Nedergaard M. (2019). Astrocytes in chronic pain and itch. Nat Rev Neurosci, 20(11), 667–685. doi:10.1038/s41583-019-0218-1 [PubMed: 31537912]

Kahanovitch U, Cuddapah VA, Pacheco NL, Holt LM, Mulkey DK, Percy AK, & Olsen ML (2018). MeCP2 Deficiency Leads to Loss of Glial Kir4.1. eNeuro, 5(1). doi:10.1523/eneuro.0194-17.2018

Kanehisa M, & Goto S. (2000). KEGG: kyoto encyclopedia of genes and genomes. Nucleic Acids Res, 28(1), 27–30. doi:10.1093/nar/28.1.27 [PubMed: 10592173]

Kifayathullah LA, Arunachalam JP, Bodda C, Agbemenyah HY, Laccone FA, & Mannan AU (2010). MeCP2 mutant protein is expressed in astrocytes as well as in neurons and localizes in the nucleus. Cytogenet Genome Res, 129(4), 290–297. doi:10.1159/000315906 [PubMed: 20625242]

Koyanagi S, Kusunose N, Taniguchi M, Akamine T, Kanado Y, Ozono Y, . . . Ohdo S. (2016). Glucocorticoid regulation of ATP release from spinal astrocytes underlies diurnal exacerbation of neuropathic mechanical allodynia. Nat Commun, 7, 13102. doi:10.1038/ncomms13102 [PubMed: 27739425]

Liu S, Liu YP, Song WB, & Song XJ (2013). EphrinB-EphB receptor signaling contributes to bone cancer pain via Toll-like receptor and proinflammatory cytokines in rat spinal cord. Pain, 154(12), 2823–2835. doi:10.1016/j.pain.2013.08.017 [PubMed: 23973554]

MacAulay N. (2020). Molecular mechanisms of K(+) clearance and extracellular space shrinkage-Glia cells as the stars. Glia, 68(11), 2192–2211. doi:10.1002/glia.23824 [PubMed: 32181522]

Macosko EZ, Basu A, Satija R, Nemesh J, Shekhar K, Goldman M, . . . McCarroll SA. (2015). Highly Parallel Genome-wide Expression Profiling of Individual Cells Using Nanoliter Droplets. Cell, 161(5), 1202–1214. doi:10.1016/j.cell.2015.05.002 [PubMed: 26000488]

Manners MT, Tian Y, Zhou Z, & Ajit SK (2015). MicroRNAs downregulated in neuropathic pain regulate MeCP2 and BDNF related to pain sensitivity. FEBS Open Bio, 5, 733–740. doi:10.1016/j.fob.2015.08.010

Nam Y, Kim JH, Kim JH, Jha MK, Jung JY, Lee MG, . . . Suk K. (2016). Reversible Induction of Pain Hypersensitivity following Optogenetic Stimulation of Spinal Astrocytes. Cell Rep, 17(11), 3049–3061. doi:10.1016/j.celrep.2016.11.043 [PubMed: 27974216]

Naranjo C, Del Reguero L, Moratalla G, Hercberg M, Valenzuela M, & Failde I. (2019). Anxiety, depression and sleep disorders in patients with diabetic neuropathic pain: a systematic review. Expert Rev Neurother, 19(12), 1201–1209. doi:10.1080/14737175.2019.1653760 [PubMed: 31393191]

Ng CH, & Ong WY (2001). Increased expression of gamma-aminobutyric acid transporters GAT-1 and GAT-3 in the spinal trigeminal nucleus after facial carrageenan injections. Pain, 92(1–2), 29–40. doi:10.1016/s0304-3959(00)00468-1 [PubMed: 11323124]

Nguyen PT, Dorman LC, Pan S, Vainchtein ID, Han RT, Nakao-Inoue H, . . . Molofsky AV. (2020). Microglial Remodeling of the Extracellular Matrix Promotes Synapse Plasticity. Cell, 182(2), 388–403.e315. doi:10.1016/j.cell.2020.05.050 [PubMed: 32615087]

Nwaobi SE, Cuddapah VA, Patterson KC, Randolph AC, & Olsen ML (2016). The role of glial-specific Kir4.1 in normal and pathological states of the CNS. Acta Neuropathol, 132(1), 1–21. doi:10.1007/s00401-016-1553-1 [PubMed: 26961251]

Ohno Y, Kinboshi M, & Shimizu S. (2018). Inwardly Rectifying Potassium Channel Kir4.1 as a Novel Modulator of BDNF Expression in Astrocytes. Int J Mol Sci, 19(11). doi:10.3390/ijms19113313

Olsen ML, Higashimori H, Campbell SL, Hablitz JJ, & Sontheimer H. (2006). Functional expression of Kir4.1 channels in spinal cord astrocytes. Glia, 53(5), 516–528. doi:10.1002/glia.20312 [PubMed: 16369934]

Orefice LL, Zimmerman AL, Chirila AM, Sleboda SJ, Head JP, & Ginty DD (2016). Peripheral Mechanosensory Neuron Dysfunction Underlies Tactile and Behavioral Deficits in Mouse Models of ASDs. Cell, 166(2), 299–313. doi:10.1016/j.cell.2016.05.033 [PubMed: 27293187]

Rimmele TS, Rocher AB, Wellbourne-Wood J, & Chatton JY (2017). Control of Glutamate Transport by Extracellular Potassium: Basis for a Negative Feedback on Synaptic Transmission. Cereb Cortex, 27(6), 3272–3283. doi:10.1093/cercor/bhx078 [PubMed: 28369311]

Rose CR, Ziemens D, & Verkhratsky A. (2020). On the special role of NCX in astrocytes: Translating Na(+)-transients into intracellular Ca(2+) signals. Cell Calcium, 86, 102154. doi:10.1016/j.ceca.2019.102154

Ruscheweyh R, & Sandkühler J. (2002). Lamina-specific membrane and discharge properties of rat spinal dorsal horn neurones in vitro. J Physiol, 541(Pt 1), 231–244. doi:10.1113/jphysiol.2002.017756 [PubMed: 12015432]

Sathyamurthy A, Johnson KR, Matson KJE, Dobrott CI, Li L, Ryba AR, . . . Levine AJ. (2018). Massively Parallel Single Nucleus Transcriptional Profiling Defines Spinal Cord Neurons and Their Activity during Behavior. Cell Rep, 22(8), 2216–2225. doi:10.1016/j.celrep.2018.02.003 [PubMed: 29466745]

Skolnick P. (2018). The Opioid Epidemic: Crisis and Solutions. Annu Rev Pharmacol Toxicol, 58, 143–159. doi:10.1146/annurev-pharmtox-010617-052534 [PubMed: 28968188]

Smrt RD, Eaves-Egenes J, Barkho BZ, Santistevan NJ, Zhao C, Aimone JB, . . . Zhao X. (2007). Mecp2 deficiency leads to delayed maturation and altered gene expression in hippocampal neurons. Neurobiol Dis, 27(1), 77–89. doi:10.1016/j.nbd.2007.04.005 [PubMed: 17532643]

Sobrinho CR, Gonçalves CM, Takakura AC, Mulkey DK, & Moreira TS (2017). Fluorocitrate-mediated depolarization of astrocytes in the retrotrapezoid nucleus stimulates breathing. J Neurophysiol, 118(3), 1690–1697. doi:10.1152/jn.00032.2017 [PubMed: 28679838]

Sommer C, Leinders M, & Üçeyler N. (2018). Inflammation in the pathophysiology of neuropathic pain. Pain, 159(3), 595–602. doi:10.1097/j.pain.0000000000001122 [PubMed: 29447138]

Suzuki A, Shinoda M, Honda K, Shirakawa T, & Iwata K. (2016). Regulation of transient receptor potential vanilloid 1 expression in trigeminal ganglion neurons via methyl-CpG binding protein 2 signaling contributes tongue heat sensitivity and inflammatory hyperalgesia in mice. Mol Pain, 12. doi:10.1177/1744806916633206

Tajerian M, Alvarado S, Millecamps M, Vachon P, Crosby C, Bushnell MC, . . . Stone LS. (2013). Peripheral nerve injury is associated with chronic, reversible changes in global DNA methylation in the mouse prefrontal cortex. PLoS One, 8(1), e55259. doi:10.1371/journal.pone.0055259

Tao W, Chen C, Wang Y, Zhou W, Jin Y, Mao Y, . . . Zhang Z. (2020). MeCP2 mediates transgenerational transmission of chronic pain. Prog Neurobiol, 189, 101790. doi:10.1016/j.pneurobio.2020.101790

Tochiki KK, Cunningham J, Hunt SP, & Géranton SM (2012). The expression of spinal methyl-CpG-binding protein 2, DNA methyltransferases and histone deacetylases is modulated in persistent pain states. Mol Pain, 8, 14. doi:10.1186/1744-8069-8-14 [PubMed: 22369085]

Tsantoulas C, & McMahon SB (2014). Opening paths to novel analgesics: the role of potassium channels in chronic pain. Trends Neurosci, 37(3), 146–158. doi:10.1016/j.tins.2013.12.002 [PubMed: 24461875]

Vit JP, Ohara PT, Bhargava A, Kelley K, & Jasmin L. (2008). Silencing the Kir4.1 potassium channel subunit in satellite glial cells of the rat trigeminal ganglion results in pain-like behavior in the absence of nerve injury. J Neurosci, 28(16), 4161–4171. doi:10.1523/jneurosci.5053-07.2008 [PubMed: 18417695]

Wahlman C, Doyle TM, Little JW, Luongo L, Janes K, Chen Z, . . . Salvemini D. (2018). Chemotherapy-induced pain is promoted by enhanced spinal adenosine kinase levels through astrocyte-dependent mechanisms. Pain, 159(6), 1025–1034. doi:10.1097/j.pain.0000000000001177 [PubMed: 29419652]

Wang F, Smith NA, Xu Q, Fujita T, Baba A, Matsuda T, . . . Nedergaard M. (2012). Astrocytes modulate neural network activity by Ca^2+-dependent uptake of extracellular K+. Sci Signal, 5(218), ra26. doi:10.1126/scisignal.2002334

Wercberger R, Braz JM, Weinrich JA, & Basbaum AI (2021). Pain and itch processing by subpopulations of molecularly diverse spinal and trigeminal projection neurons. Proc Natl Acad Sci U S A, 118(28). doi:10.1073/pnas.2105732118

Xu Q, Ford NC, He S, Huang Q, Anderson M, Chen Z, . . . Dong X. (2021). Astrocytes contribute to pain gating in the spinal cord. Sci Adv, 7(45), eabi6287. doi:10.1126/sciadv.abi6287

Zachariah RM, Olson CO, Ezeonwuka C, & Rastegar M. (2012). Novel MeCP2 isoform-specific antibody reveals the endogenous MeCP2E1 expression in murine brain, primary neurons and astrocytes. PLoS One, 7(11), e49763. doi:10.1371/journal.pone.0049763

Zhang D, Wei Y, Liu J, Yang Y, Ou M, Chen Y, . . . Zhou C. (2022). Single-nucleus transcriptomic analysis reveals divergence of glial cells in peripheral somatosensory system between human and mouse. bioRxiv.

Zhang H, Mei X, Zhang P, Ma C, White FA, Donnelly DF, & Lamotte RH (2009). Altered functional properties of satellite glial cells in compressed spinal ganglia. Glia, 57(15), 1588–1599. doi:10.1002/glia.20872 [PubMed: 19330845]

Zhang R, Huang M, Cao Z, Qi J, Qiu Z, & Chiang LY (2015). MeCP2 plays an analgesic role in pain transmission through regulating CREB / miR-132 pathway. Mol Pain, 11, 19. doi:10.1186/s12990-015-0015-4 [PubMed: 25885346]

Zhang X, & Li G. (2019). P2Y receptors in neuropathic pain. Pharmacol Biochem Behav, 186, 172788. doi:10.1016/j.pbb.2019.172788

Zhang Z, Tao W, Hou Y, Wang W, Kenny P, & Pan ZJTJ S. f. N o. n. t. o. j. o. t. (2014). MeCP2 repression of G9a in regulation of pain and morphine reward. 34(27), 9076–9087. doi:10.1523/jneurosci.4194-13.2014

Zhou C, Ke B, Zhao Y, Liang P, Liao D, Li T, . . . Chen X. (2015). Hyperpolarization-activated cyclic nucleotide-gated channels may contribute to regional anesthetic effects of lidocaine. Anesthesiology, 122(3), 606–618. doi:10.1097/aln.0000000000000557 [PubMed: 25485469]

Highlights

- Astrocytic MeCP2 regulates expression of Kir4.1 in the spinal dorsal cord.
- Decreased Kir4.1 changes the astrocytic excitability and firing patterns of neurons.
- Spinal Kir4.1 may be a new target for treatment of chronic neuropathic pain.

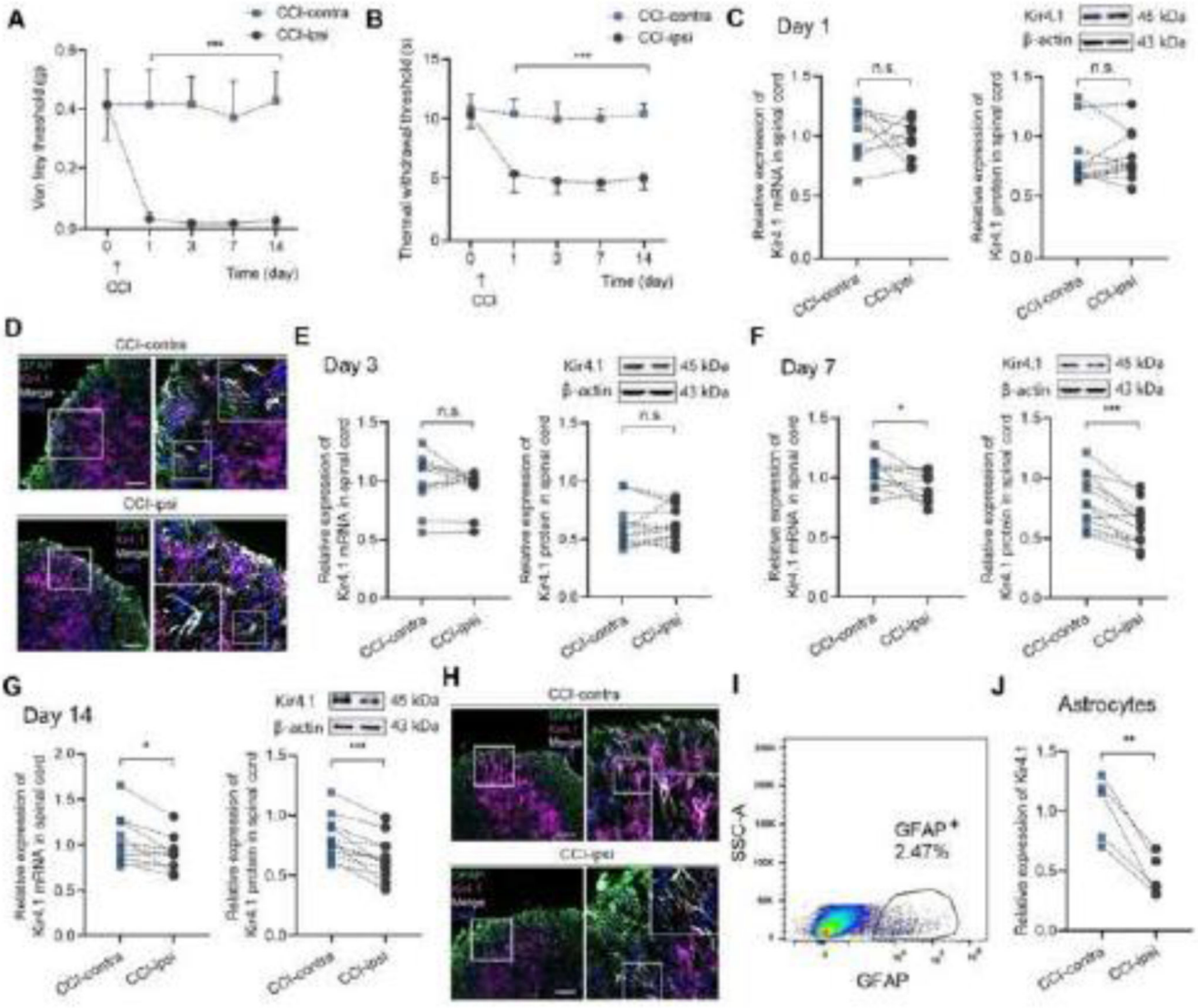

Fig. 1:

Expression of Kir4.1 decreases one week after CCI in the spinal cord. **(A-B)** CCI induced mechanical **(A)** and thermal **(B)** hyperalgesia in adult (wild type, C57BL/6 J) mice (n = 20, male = 10, female = 10). **(C, E)** Kir4.1 mRNA (left, by RT-PCR, n = 10, male = 5, female = 5) and expression of Kir4.1 protein (right, by Western blot, n = 12, male = 6, female = 6) did not change on day 1 **(C)** or day 3 **(E)** after CCI in the CCI-ipsi side of the spinal lumbar enlargement. **(D)** Fluorescent images of spinal lumbar enlargement sections from CCI-contra and CCI-ipsi show the expression of GFAP (green) and Kir4.1 (purple) on day 1 after CCI. The image on the right depicts the area shown in the boxes of the left image. **(F-G)** Kir4.1 mRNA (left, by RT-PCR, n = 10, male = 5, female = 5) and protein (right, by Western blot, n = 12, male = 6, female = 6) expression decreased on day 7 **(F)** and day 14 **(G)** after CCI in the CCI-ipsi side of the spinal lumbar enlargement. **(H)** Fluorescent images of spinal lumbar enlargement sections from CCI-contra and CCI-ipsi show the expression of GFAP (green) and Kir4.1 (purple) on day 14 after CCI. The image on the right depicts

the area shown in the boxes of the left image. **(I)** FACS plots showing the sorting gates and antibodies that were used for isolation of astrocytes on the day 14 after CCI. **(J)** Kir4.1 mRNA in FACS-enriched astrocytes was decreased on day 14 after CCI in the CCI-ipsi side of the spinal lumbar enlargement (n = 5, male = 3, female = 2).

Scale bar: 100 μm. Data are presented as mean ± SD. n.s., not significant; * $P < 0.05$, ** $P < 0.01$, *** $P < 0.001$, by two-way ANOVA (A, B) and/or paired t-test (C, E, F, G, J).

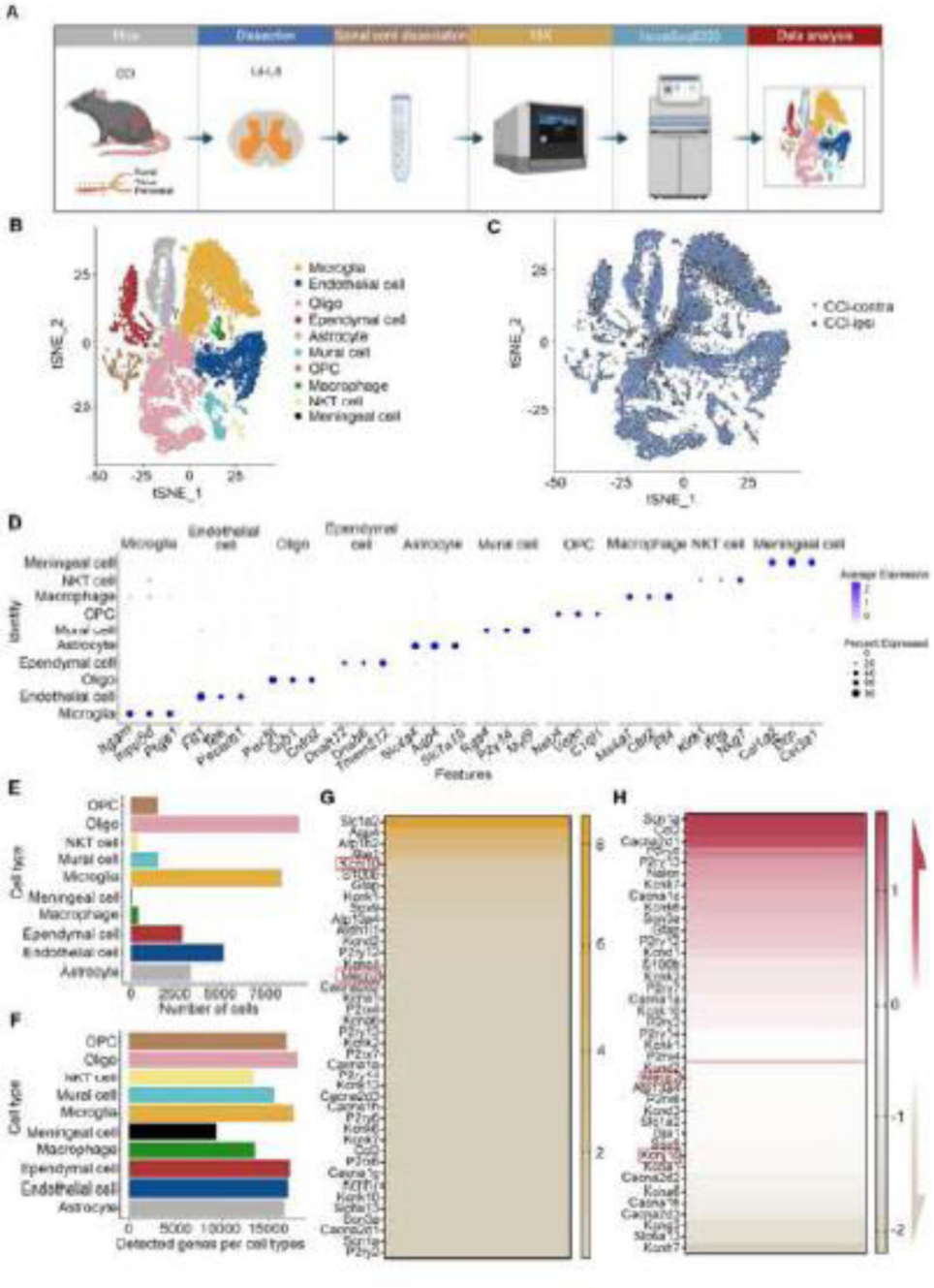

Fig. 2:

Identification of gene expression changes in astrocytes on day 14 after CCI by scRNA-seq. **(A)** Overview of the experimental workflow. **(B)** TSNE plot depicting 27,188 single cells from the CCI-contra and CCI-ipsi sides of the spinal lumbar enlargement on day 14 after CCI. **(C)** Global analysis showing the distribution of cells between the CCI-ipsi and CCI-contra. **(D)** The distribution of expression levels of well-known representative cell-type-enriched marker genes across all 10 cell types. The size of the circle reflects the proportion of the cells expressing the marker gene in a cluster, and the color intensity

reflects its average expression level within that cluster. **(E-F)** Bar plot showing the total number of detected cells **(E)** and the total number of detected genes per cell type **(F)**. **(G)** Examples of average expression in genes which are commonly expressed in astrocytes. **(H)** Examples of fold changes in the expression of genes (which are commonly expressed in astrocytes) between CCI-ipsi and CCI-contra samples on day 14 after CCI.

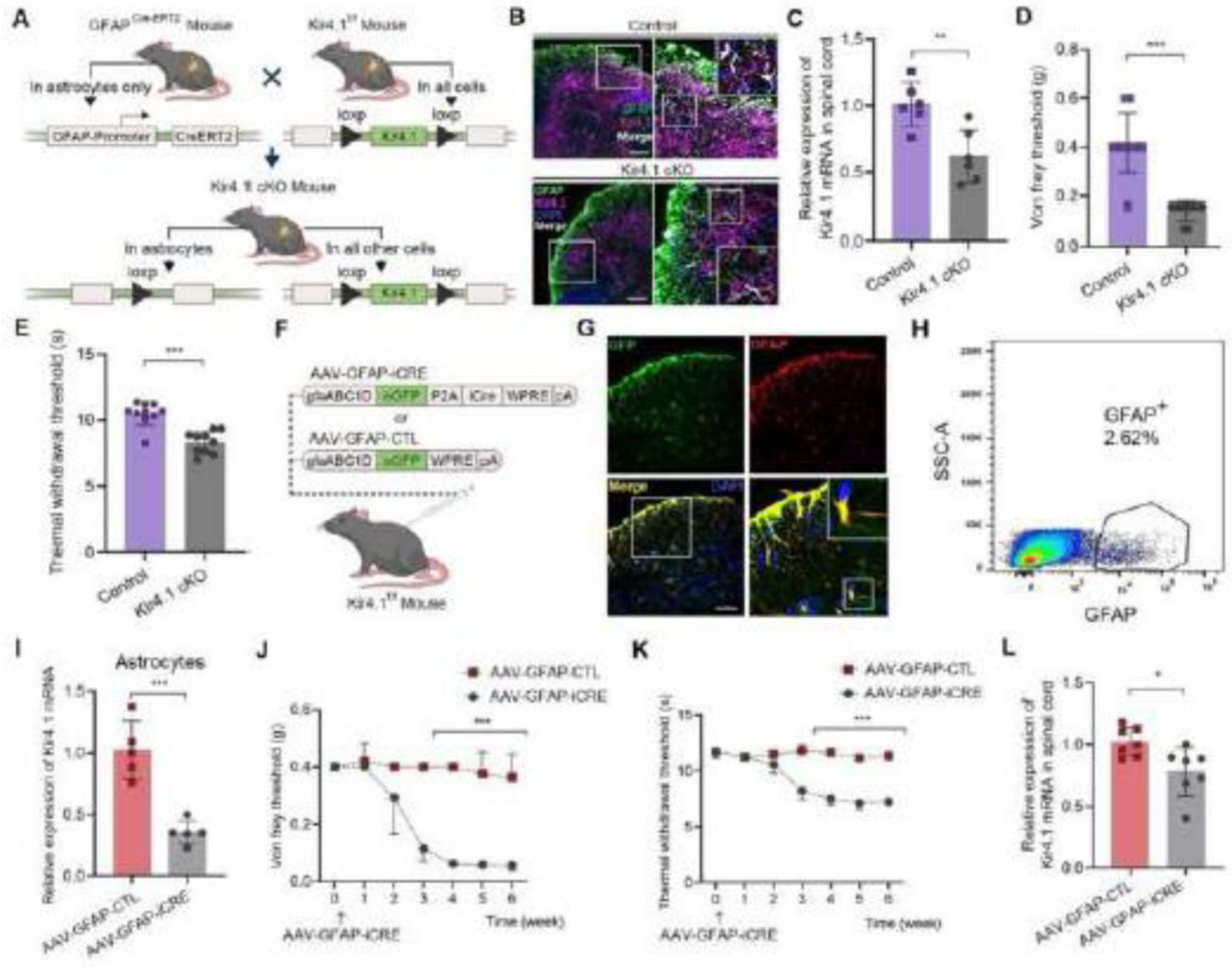

Fig. 3:

Conditional knockout of Kir4.1 in astrocytes induces pain hypersensitivity in mice. **(A)** Schematic of the generation of conditional Kir4.1 knockout mice ($GFAP^{Cre\text{-}ERT2}$::$Kir4.1^{f/f}$; AKA Kir4.1 cKO). **(B)** Fluorescent images of spinal lumbar enlargement sections from control (top) and Kir4.1 cKO mice (bottom) stained for GFAP (green) and Kir4.1 (purple). The image on the right depicts the area in the boxes on the left image. **(C)** Kir4.1 mRNA was decreased in spinal lumbar enlargement of Kir4.1 cKO mice (n = 6, male = 3, female = 3). **(D-E)** Deletion of Kir4.1 in astrocytes led to hyperalgesia in both mechanical **(D)** and thermal **(E)** sensations (n=10, male = 5, female = 5). **(F)** Schematic paradigm of knockdown Kir4.1 in spinal cord by injecting AAV-GFAP-iCRE in $Kir4.1^{f/f}$ mice. AAV vectors were engineered to express eGFP-Cre or an eGFP-control under a GFAP promoter in $Kir4.1^{f/f}$ mice. **(G)** Fluorescent images in spinal lumbar enlargement four weeks after intrathecal injection of AAV-GFAP-iCRE in $Kir4.1^{f/f}$ mice. The image on the right depicts the area shown in the boxes of the left image. **(H)** FACS plots showing the sorting gates and antibodies that were used for isolation of astrocytes after intrathecal injection of AAV-

GFAP-iCRE in Kir4.1$^{f/f}$ mice. **(I)** Kir4.1 mRNA in astrocytes (by FACS cell sorting) was significantly decreased in AAV-GFAP-iCRE-injected mice (n = 5, male = 3, female = 2). **(J-K)** Mechanical **(J)** and thermal **(K)** hyperalgesia was found in Kir4.1$^{f/f}$ mice 4 weeks after AAV-GFAP-iCRE intrathecal injection (n = 10, male = 5, female = 5). **(L)** Statistical data of Kir4.1 mRNA in spinal lumbar enlargement 6 weeks after intrathecal injection of AAV-GFAP-CTL and AAV-GFAP-iCRE in Kir4.1$^{f/f}$ mice (n = 7, male = 3, female = 4). Scale bar: 100 μm. Data are presented as mean ± SD. * $P < 0.05$, ** $P < 0.01$, *** $P < 0.001$ by Wilcoxon test (C, D), unpaired t-test (E, I, L) and two-way ANOVA (J, K).

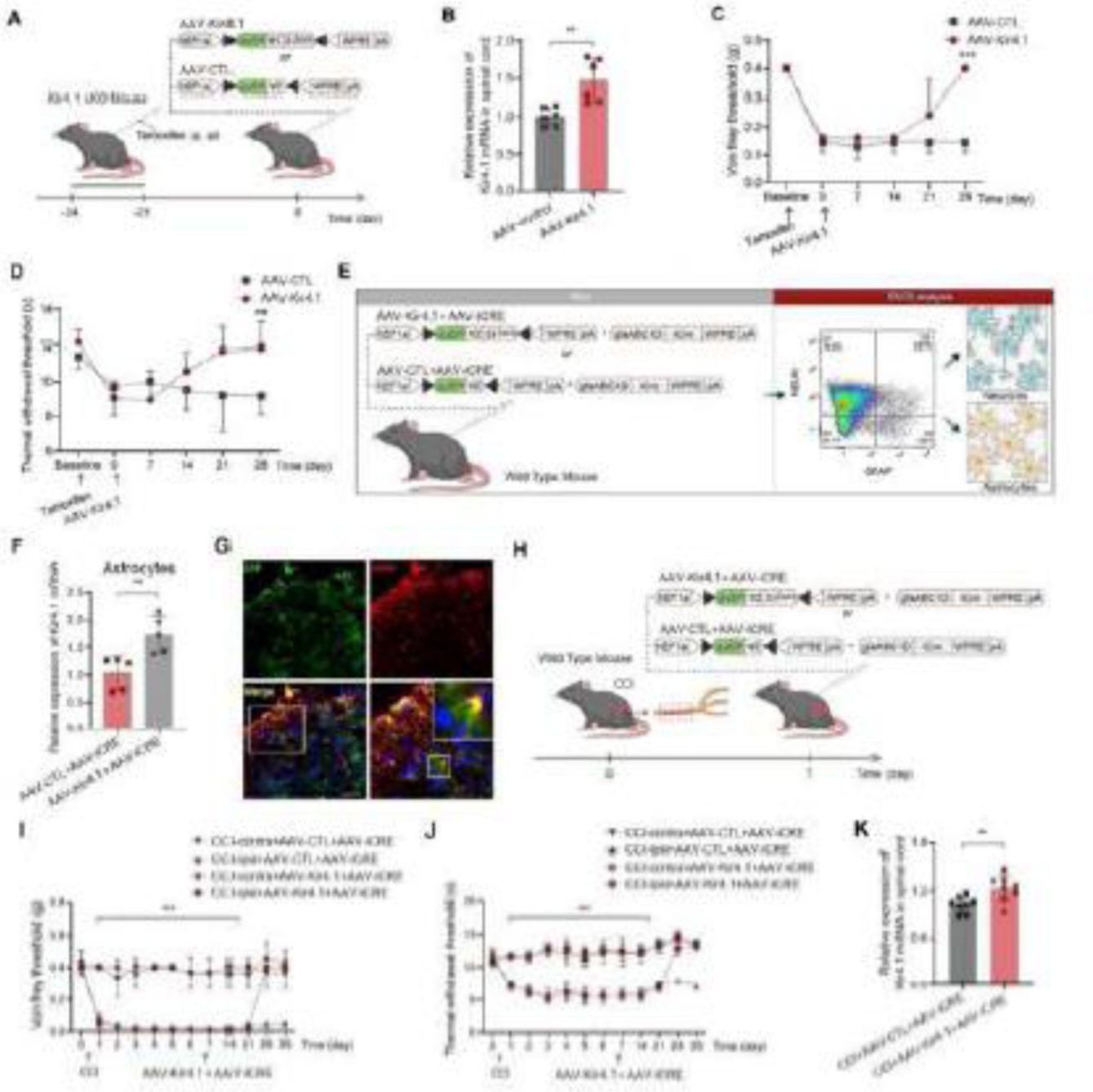

Fig. 4:

Overexpression of Kir4.1 can relieve hyperalgesia behaviors in both Kir4.1 cKO mice and CCI mice. **(A)** Experimental paradigm of behavioral test and injection of viral constructs in Kir4.1 cKO mice. AAV vectors were engineered to overexpress Kir4.1 or an eGFP control in Kir4.1 cKO mice. **(B)** The expression of Kir4.1 in spinal cord was increased after overexpression of Kir4.1 in spinal cord of Kir4.1 cKO mice, confirmed by RT-PCR (n = 6, male = 3, female = 3). **(C-D)** The mechanical **(C)** and thermal **(D)** hyperalgesia responses were completely relieved to normal levels after intrathecal injection of AAV-Kir4.1 in the

Kir4.1 cKO mice; AAV-CTL (control) did not produce a therapeutic effect (n = 6, male = 3, female = 3). **(E)** Workflow diagram depicting the FACS protocol to dissociate and sort neurons and astrocytes. **(F)** The expression of Kir4.1 mRNA increased in astrocytes after specifically overexpressing Kir4.1 in astrocytes in Kir4.1 cKO mice (n = 5, male = 2, female = 3). **(G)** Fluorescent images of spinal cord after injection of AAV-Kir4.1. The image on the right depicts the area shown in the boxes of the left image. **(H)** Experimental paradigm of the behavioral test and injection of viral constructs in CCI mice. AAV vectors were engineered to overexpress Kir4.1 (AAV-Kir4.1 and AAV-iCRE at a 1:1 ratio) and a control (AAV-CTL and AAV-iCRE at a 1:1 ratio) under a GFAP promoter. **(I-J)** Overexpression of Kir4.1 completely rescued the CCI-induced mechanical **(I)** and thermal **(J)** hyperalgesia in adult wild-type mice (n = 7, male = 4, female = 3). (**K)** The expression of Kir4.1 was increased after intrathecal injection of AAV-Kir4.1 in spinal cord of wild-type mice after CCI (n = 8, male = 4, female = 4). Scale bars: 100 μm. Data are presented as mean ± SD. $^{**}P < 0.01$, $^{***}P < 0.001$ by two-way ANOVA (C, D, I, J) and unpaired t-test (B, F, K).

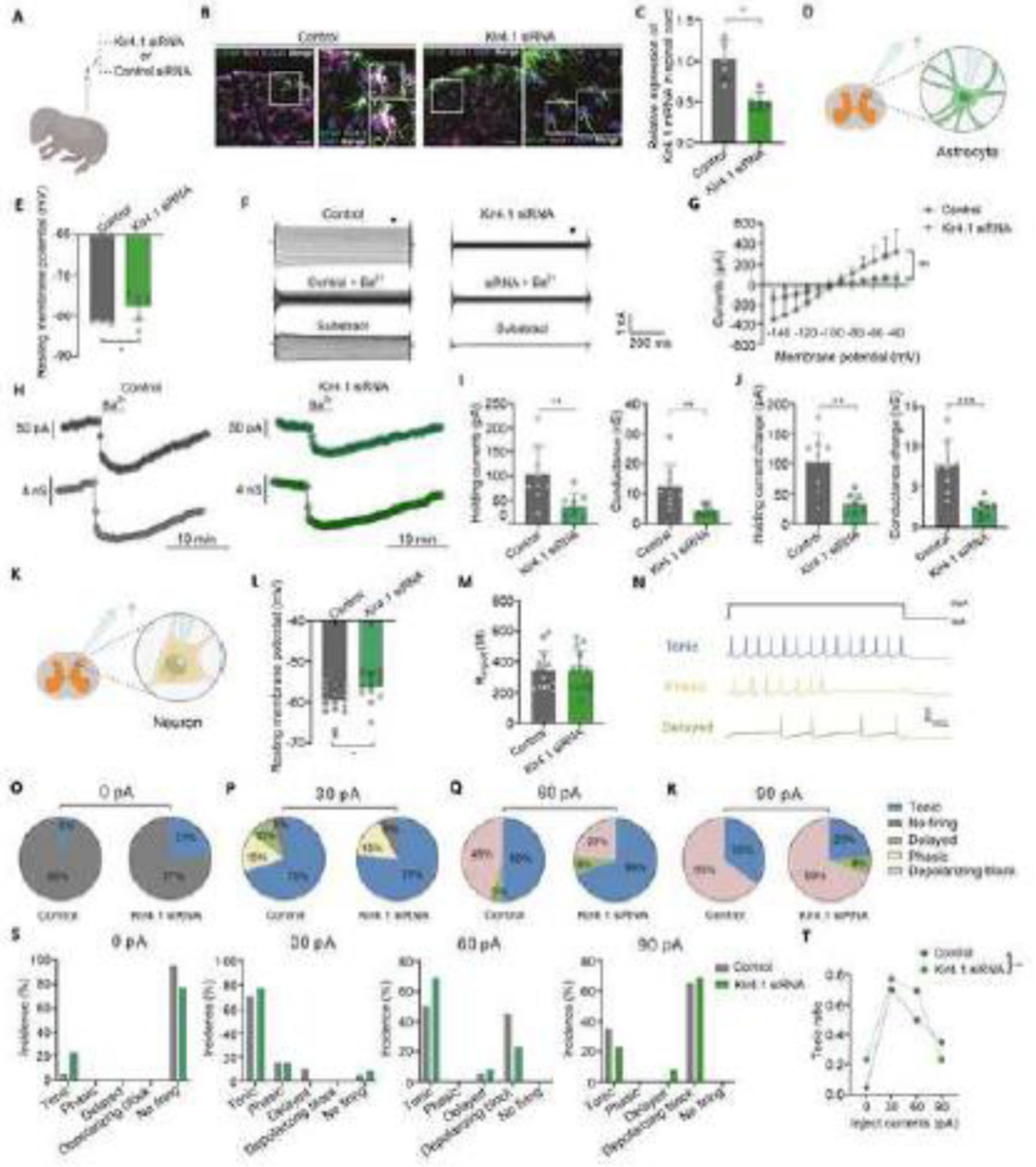

Fig. 5:

Kir4.1-siRNA was used to knockdown the expression of Kir4.1 in spinal cord of neonatal mice, for spinal slice patch-clamp recording. **(A)** Schematic paradigm of the Kir4.1-siRNA injection in spinal cord of pups. **(B)** Fluorescent images of spinal cord after injection of control-siRNA (left) and Kir4.1-siRNA (right). The image on the right depicts the area shown in the boxes of the left image. **(C)** Compared to the control-siRNA, the level of Kir4.1 mRNA was decreased in spinal cord injected with Kir4.1-siRNA (n = 5). **(D)** Schematic paradigm of recordings on astrocytes in the dorsal horn of spinal cord. **(E)**

Astrocytic knockdown of Kir4.1 depolarized RMPs in dorsal horn astrocytes in the spinal cord slice (control-siRNA: n = 5, Kir4.1-siRNA: n = 7). **(F)** Traces of the current-voltage relationship between –40 and –150 mV from a holding potential of –80 mV, under control (5% CO_2 + 95% O_2) and 100 μm $BaCl_2$ conditions. Dots above current traces indicate where measurements were taken to construct the I-V relationships. **(G)** I-V plot representing the Ba^{2+}-sensitive currents in astrocytes of control-siRNA- and Kir4.1-siRNA-treated mice in P10-P14 (n = 9). **(H)** Traces of holding current (top) and conductance (bottom) from control-siRNA (left) and Kir4.1-siRNA (right) animals exposed to 100 μm $BaCl_2$. **(I)** Summary data show the effects of knockdown of Kir4.1 on holding current and conductance in control-siRNA and Kir4.1-siRNA mice (n = 9). **(J)** Summary plots show that 100 μM Ba^{2+} inhibited the holding current and conductance in control-siRNA and Kir4.1-siRNA mice (n = 8). **(K)** Schematic paradigm of patch clamp recordings on neurons in the dorsal horn of spinal cord. **(L)** Astrocytic knockdown of Kir4.1-depolarized RMPs in neurons of spinal lamina I and II (control-siRNA: n = 13, Kir4.1-siRNA: n = 18). **(M)** There is no difference in neuronal R_{input} between control-siRNA- and Kir4.1-siRNA-treated mice (n = 13)**. (N)** Three firing patterns distinguished by properties of AP discharge. **(O-S)** The incidence of the four different firing patterns under 0-pA **(O, S left)**, 30-pA **(P, S middle left)**, 60-pA **(Q, S middle right)** and 90-pA **(R, S right)** injections in spinal lamina I and II neurons of control-siRNA and Kir4.1-siRNA mice. **(T)** The tonic firing pattern ratio between control-siRNA and Kir4.1-siRNA mice under 0-pA, 30-pA, 60-pA and 90-pA current injections. Scale bars: 100 μm. Data are presented as mean ± SD. $*P < 0.05$, $**P < 0.01$, $***P < 0.001$ by unpaired t-test (C, E, I, J, L, M), two-way ANOVA (G) and Cochran–Armitage trend test (T).

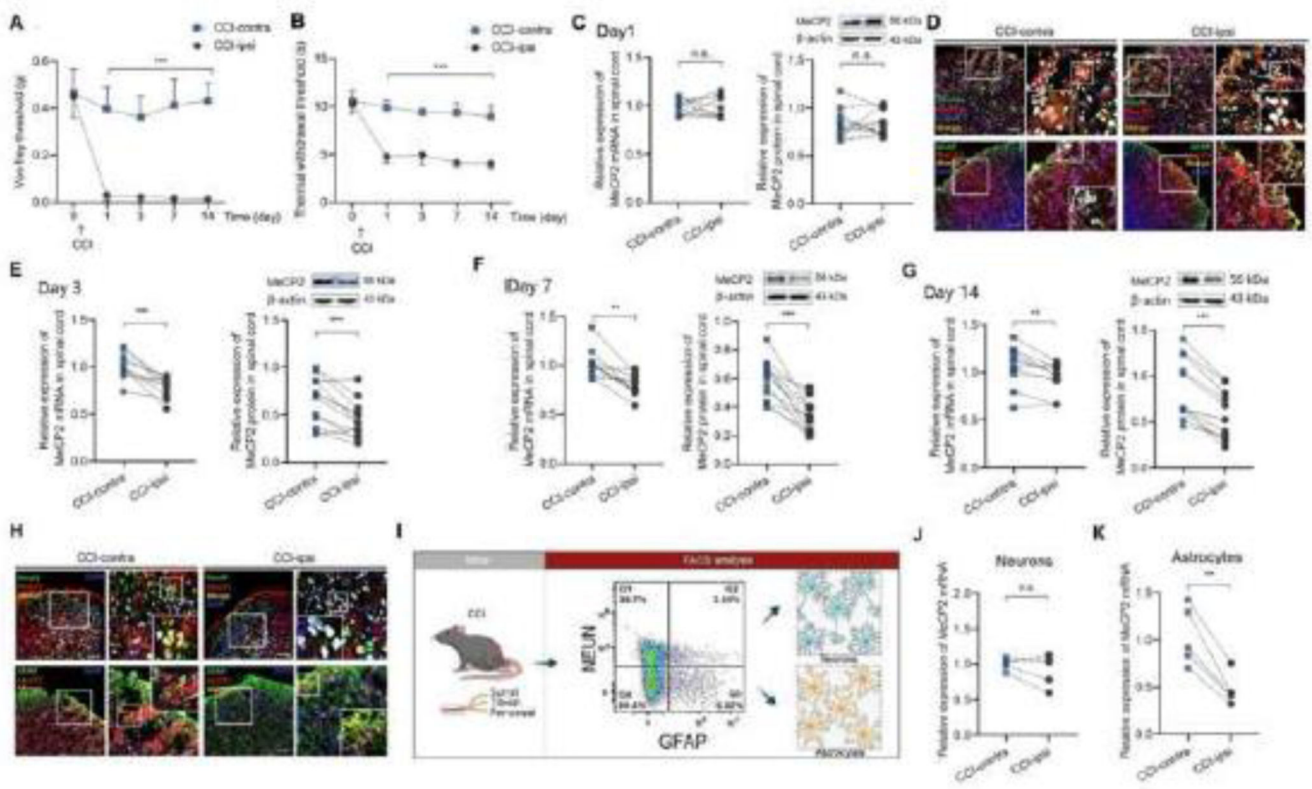

Fig. 6:

Expression of MeCP2 decreases 3 days after CCI in the spinal cord. **(A-B)** CCI induced mechanical **(A)** and thermal **(B)** pain in adult (wild type, C57BL/6 J) mice (n = 12, male = 6, female = 6). **(C)** MeCP2 mRNA (left, by RT-PCR, n = 10, male = 5, female = 5) and protein (right, by Western blot, n = 12, male = 6, female = 6) expression was unchanged on day 1 after CCI in the CCI-ipsi side of the spinal lumbar enlargement. **(D)** Fluorescent images of spinal lumbar enlargement sections from CCI-contra and CCI-ipsi show the expression of NeuN and MeCP2 (top) and GFAP and MeCP2 (bottom) on day 1. The image on the right depicts the area shown in the boxes of the left image. **(E-G)** MeCP2 mRNA (by RT-PCR, n = 10, male = 5, female = 5) and protein (right, by Western blot, n = 12, male = 6, female = 6) expression was significantly decreased on day 3 **(E)**, day 7 **(F)**, and day 14 **(G)** after CCI in the CCI-ipsi side of the spinal lumbar enlargement. **(H)** Fluorescent images of spinal lumbar enlargement sections from CCI-contra and CCI-ipsi show the expression of NeuN and MeCP2 (top) and GFAP and MeCP2 (bottom) on day 14. The image on the right depicts the area shown in the boxes of the left image. **(I)** Workflow diagram depicting the FACS protocol to dissociate and sort neurons and astrocytes after CCI. **(J-K)** The expression of MeCP2 mRNA were unchanged in neurons **(J)** while decreased in astrocytes **(K)** on day 14 after CCI in the CCI-ipsi side of the spinal lumbar enlargement (n = 5, male = 2, female = 3). Scale bar: 100 μm. Data are presented as mean ± SD. $^{**}P < 0.01$, $^{***}P < 0.001$ by two-way ANOVA (A, B) and paired t-test (C, E, F, G, J, K).

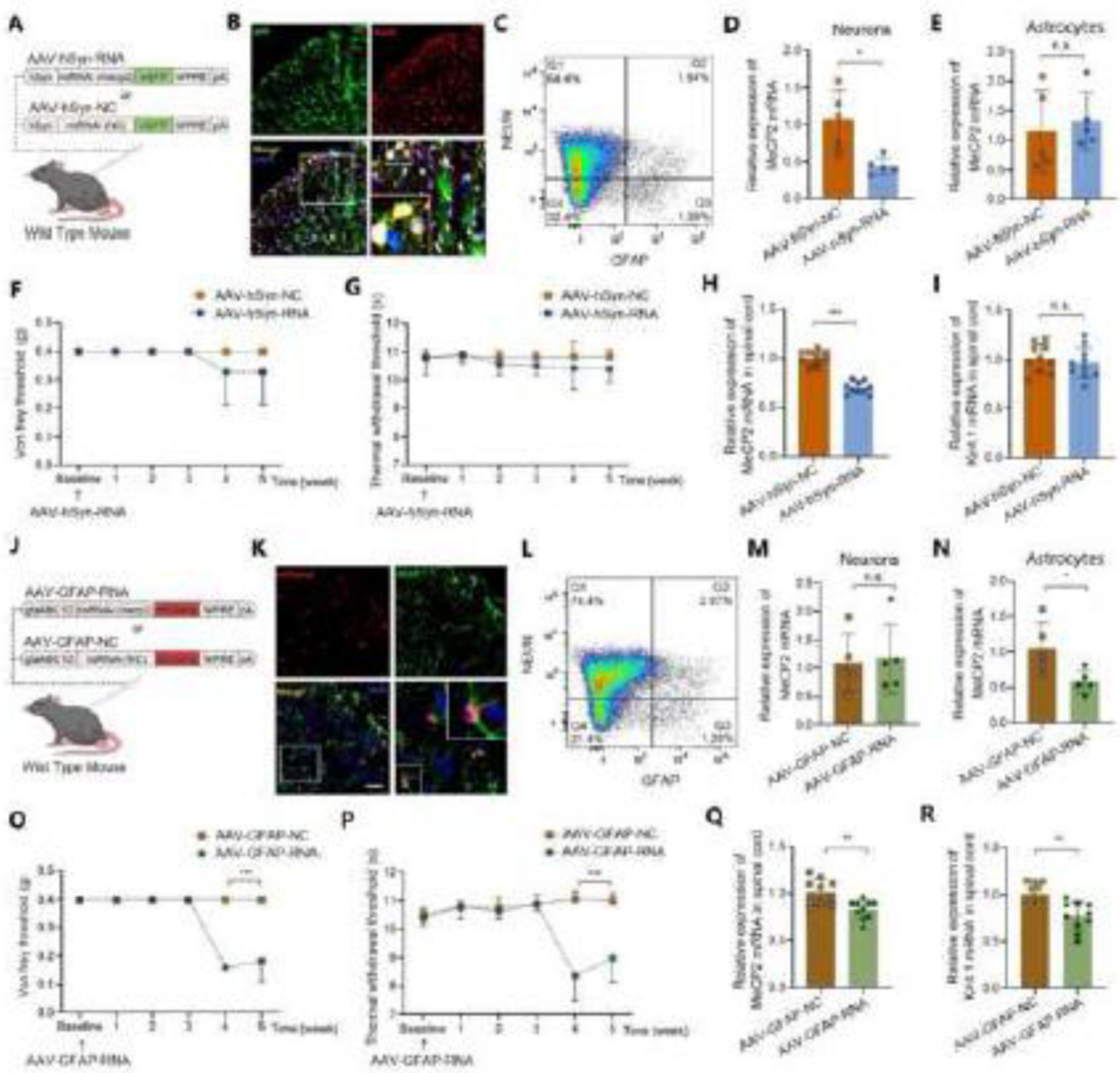

Fig. 7:

Astrocyte-specific knockdown of MeCP2 induces hyperalgesia in mice. **(A)** Schematic paradigm of knocking down MeCP2 in neurons in wild-type mice. AAV vectors were engineered to express MeCP2 RNAi (top) or a control construct (bottom) in neurons. **(B)** Fluorescent images of AAV-hSyn-RNA 4 weeks after injection. The image on the right depicts the area shown in the boxes of the left image. **(C)** Representative flow cytometric data after intrathecal injection of AAV-hSyn-RNA. **(D-E)** The expression of MeCP2 mRNA in neurons was significantly decreased **(D)** while no change was found in astrocytes **(E)** when using FACS to sort neurons and astrocytes (n = 5, male = 3, female = 2). **(F-G)** No significant mechanical **(F)** or thermal **(G)** hyperalgesia was found after intrathecal injection

of AAV-hSyn-RNA, which selectively knocks down expression of MeCP2 in neurons (n = 10, male = 5, female = 5). **(H)** The expression of MeCP2 was decreased after intrathecal injection of AAV-hSyn-RNA (n = 10, male = 5, female = 5). **(I)** Kir4.1 mRNA levels were unchanged after intrathecal injection of AAV-hSyn-RNA in spinal cord (n = 10, male = 5, female = 5). **(J)** Schematic paradigm of our strategy to specifically knockdown MeCP2 in astrocytes in wild-type mice. The AAV vectors were engineered to express MeCP2 RNAi (top) or a control construct (bottom) in astrocytes. **(K)** Fluorescent images of AAV-GFAP-RNA 4 weeks after injection. The image on the right depicts the area shown in the boxes of the left image. **(L)** Representative flow cytometric data after intrathecal injection of AAV-GFAP-RNA. **(M-N)** The expression of MeCP2 was significantly decreased in astrocytes **(N)** while no change was found in neurons **(M)** after intrathecal injection of AAV-GFAP-RNA, confirmed by RT-PCR (n = 5, male = 3, female = 2). **(O-P)** The mice developed mechanical **(O)** and thermal **(P)** hyperalgesia after intrathecal injection of AAV-GFAP-RNA, which selectively knocks down expression of MeCP2 in astrocytes (n = 10, male = 5, female = 5). **(Q)** The expression of MeCP2 was decreased in spinal cord after intrathecal injection of AAV-GFAP-RNA, confirmed by RT-PCR (n = 10, male = 5, female = 5). **(R)** Similarly, Kir4.1 mRNA was decreased after intrathecal injection of AAV-GFAP-RNA (n = 10, male = 5, female = 5). Scale bar: 100 μm. Data are presented as mean ± SD. n.s., not significant; $*P<0.05$; $**P < 0.01$; $***P < 0.001$ by two-way ANOVA (F, G, O, P) and unpaired t-test (D, E, H, I, M, N, Q, R).

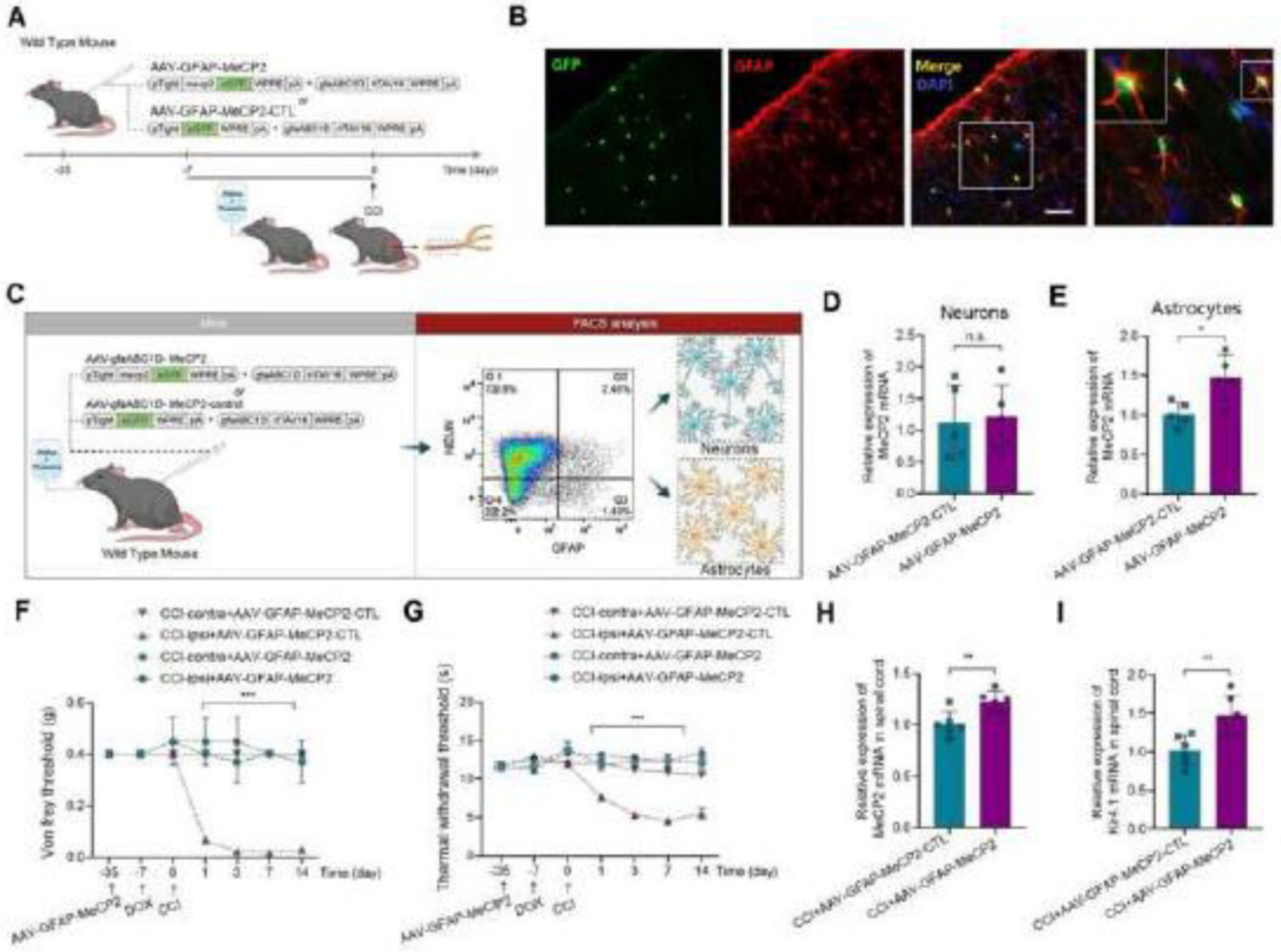

Fig. 8:

Astrocytic MeCP2 regulates Kir4.1 expression in spinal cord in CCI-induced neuropathic pain. **(A)** Schematic paradigm of overexpression of astrocytic MeCP2 after CCI in wild-type mice. AAV vectors were engineered to overexpress MeCP2 (in a 1:1 ratio) or a control construct (in a 1:1 ratio) under a GFAP promoter in wild-type mice. **(B)** Fluorescent images of AAV-GFAP-MeCP2 (green) co-stained with GFAP (red). The image on the right depicts the area shown in the boxes of the left image. **(C)** Workflow diagram depicting the FACS protocol to dissociate and sort neurons and astrocytes after overexpression of MeCP2 in spinal cord. **(D-E)** Expression of MecP2 mRNA level was significantly increased in astrocytes rather than neurons, as measured by FACS (n = 5, male =3, female = 2). **(F-G)** Overexpression of MeCP2 in astrocytes can rescue hyperalgesia behaviors after CCI (n = 8, male =4, female = 4). **(H-I)** Expression of MeCP2 was increased after injection of AAV-GFAP-MeCP2 **(H)**, consistent with the higher expression of Kir4.1 **(I)** (n = 6, male = 3, female = 3). Scale bars: 100 μm. Data are presented as mean ± SD. n.s., not significant; **P*<0.05; ***P* < 0.01; ****P* < 0.001 by two-way ANOVA (F, G) and unpaired t-test (D, E, H, I).